

AFRL-VA-WP-TR-2006-3043



**CRACK GROWTH AND STRESS
INTENSITY PREDICTION
TECHNIQUES**

**Delivery Order 0004: Implementing
Models and Libraries**

Craig Brooks, Kyle Honeycutt, and Scott Prost Domasky

**Analytical Processes/Engineered Solutions (AP/ES), Inc.
6669 Fyler Avenue
St. Louis, MO 63139**

MARCH 2006

Final Report for 01 October 2002 – 20 March 2006

Approved for public release; distribution is unlimited.

STINFO COPY

**AIR VEHICLES DIRECTORATE
AIR FORCE RESEARCH LABORATORY
AIR FORCE MATERIEL COMMAND
WRIGHT-PATTERSON AIR FORCE BASE, OH 45433-7542**

NOTICE AND SIGNATURE PAGE

Using Government drawings, specifications, or other data included in this document for any purpose other than Government procurement does not in any way obligate the U.S. Government. The fact that the Government formulated or supplied the drawings, specifications, or other data does not license the holder or any other person or corporation; or convey any rights or permission to manufacture, use, or sell any patented invention that may relate to them.

This report was cleared for public release by the Air Force Research Laboratory Wright Site (AFRL/WS) Public Affairs Office and is available to the general public, including foreign nationals.

Copies may be obtained from the Defense Technical Information Center (DTIC) (<http://www.dtic.mil>).

AFRL-VA-WP-TR-2006-3043 HAS BEEN REVIEWED AND IS APPROVED FOR PUBLICATION IN ACCORDANCE WITH ASSIGNED DISTRIBUTION STATEMENT.

**//Signature//*

James A. Harter
Program Manager
Analytical Structural Mechanics Branch

//Signature//

Kristina Langer, Ph.D.
Branch Chief
Analytical Structural Mechanics Branch

//Signature//

David M. Pratt, Ph.D.
Technical Advisor
Structures Division

This report is published in the interest of scientific and technical information exchange, and its publication does not constitute the Government's approval or disapproval of its ideas or findings.

Disseminated copies will show “//signature//*” stamped or typed above the signature blocks.

REPORT DOCUMENTATION PAGE				<i>Form Approved</i> OMB No. 0704-0188	
<p>The public reporting burden for this collection of information is estimated to average 1 hour per response, including the time for reviewing instructions, searching existing data sources, gathering and maintaining the data needed, and completing and reviewing the collection of information. Send comments regarding this burden estimate or any other aspect of this collection of information, including suggestions for reducing this burden, to Department of Defense, Washington Headquarters Services, Directorate for Information Operations and Reports (0704-0188), 1215 Jefferson Davis Highway, Suite 1204, Arlington, VA 22202-4302. Respondents should be aware that notwithstanding any other provision of law, no person shall be subject to any penalty for failing to comply with a collection of information if it does not display a currently valid OMB control number. PLEASE DO NOT RETURN YOUR FORM TO THE ABOVE ADDRESS.</p>					
1. REPORT DATE (DD-MM-YY) March 2006		2. REPORT TYPE Final		3. DATES COVERED (From - To) 10/01/2002 – 03/20/2006	
4. TITLE AND SUBTITLE CRACK GROWTH AND STRESS INTENSITY PREDICTION TECHNIQUES Delivery Order 0004: Implementing Models and Libraries				5a. CONTRACT NUMBER FA8650-04-D-3446-0004	
				5b. GRANT NUMBER	
				5c. PROGRAM ELEMENT NUMBER 0602201	
6. AUTHOR(S) Craig Brooks, Kyle Honeycutt, and Scott Prost Domasky				5d. PROJECT NUMBER A02P	
				5e. TASK NUMBER	
				5f. WORK UNIT NUMBER 0E	
7. PERFORMING ORGANIZATION NAME(S) AND ADDRESS(ES) Analytical Processes/Engineered Solutions (AP/ES), Inc. 6669 Fyler Avenue St. Louis, MO 63139				8. PERFORMING ORGANIZATION REPORT NUMBER	
9. SPONSORING/MONITORING AGENCY NAME(S) AND ADDRESS(ES) Air Vehicles Directorate Air Force Research Laboratory Air Force Materiel Command Wright-Patterson AFB, OH 45433-7542				10. SPONSORING/MONITORING AGENCY ACRONYM(S) AFRL-VA-WP	
				11. SPONSORING/MONITORING AGENCY REPORT NUMBER(S) AFRL-VA-WP-TR-2006-3043	
12. DISTRIBUTION/AVAILABILITY STATEMENT Approved for public release; distribution is unlimited.					
13. SUPPLEMENTARY NOTES PAO Case Number: AFRL/WS-06-0893, 04 April 2006. Report contains color.					
14. ABSTRACT The challenges of designing modern aircraft continue to drive the development of more advanced analytical tools; often these more advanced analytical tools themselves require development of other enabling technologies such as powerful computers and associated software. The primary historical objective of this project was to develop the infrastructure and to demonstrate that key enabling technologies such as faster and bigger personal computers, as well as database and programming software, have evolved to the point that more advanced analytical tools for analyzing the damage tolerance of aircraft structures are now possible.					
15. SUBJECT TERMS Damage Tolerance, Interactive Stress Intensity Modeling, External Stress Intensity Solutions, AFGROW					
16. SECURITY CLASSIFICATION OF:			17. LIMITATION OF ABSTRACT: SAR	18. NUMBER OF PAGES 70	19a. NAME OF RESPONSIBLE PERSON (Monitor) James A. Harter 19b. TELEPHONE NUMBER (Include Area Code) (937) 904-6771
a. REPORT Unclassified	b. ABSTRACT Unclassified	c. THIS PAGE Unclassified			

Table of Contents

1.	Executive Summary.....	1
2.	Introduction	2
2.1	Background	2
2.2	Previous Work.....	2
2.3	2005 Original Scope.....	4
2.4	2005 Revised Scope	5
2.5	Participants	5
2.6	Report Outline	5
3.	AFGROW External K-Solver: Integral Structure Plug-in Modifications	6
3.1	Objective and Description.....	6
3.2	Integral Structure--Modifications to Plug-Ins	6
3.3	Enhancements.....	9
3.4	Challenges	11
3.5	Limitations	11
3.6	Conclusions and Recommendations.....	11
4.	2-D Lug Finite Element Solutions: Cosine Bearing Load.....	12
4.1	Objective	12
4.2	Approach	12
4.3	Schematic	12
4.4	Results	14
4.5	Challenges	22
4.6	Limitations	22
4.7	Recommendations	22
5.	3-D Lug Finite Element Solutions: Distributed Springs.....	23
5.1	Objective	23
5.2	Approach	23
5.3	Schematic	23
5.4	Results	25
5.5	Challenges	26
5.6	Limitations	27
5.7	Recommendations	27
6.	Lug Boundary Condition Effects: Bearing Reactions and Interference Fits	28
6.1	Objective	28
6.2	Approach	28
6.3	Lug-Pin Model Schematics	30

6.4	Results	34
6.4.1	Radial Stress Distributions	35
6.4.2	Normal Stress From Hole Edge	36
6.5	Challenges	42
6.6	Limitations	42
6.7	Conclusions and Recommendations.....	43
6.7.1	Conclusions	43
6.7.2	Recommendations	44
7.	Support for Purdue Experimental Lug Tests	45
7.1	Objective	45
7.2	Approach	45
7.3	Results	47
7.4	Challenges	50
7.5	Limitations	50
7.6	Conclusions and Recommendations.....	50
7.6.1	Conclusions	50
7.6.2	Recommendations	51
8.	Conclusions and Recommendations	52
8.1	Conclusions	52
8.2	Recommendations	53
9.	References	54
10.	Appendix: Correlation of Experimental and Analytical Lug Stress Intensities.....	55
10.1	Introduction	55
10.2	Comparison of Bearing and Distributed Spring Boundary Conditions.....	55
10.3	Pin-to-Lug Fitting Effects	56
10.4	Recommendations for AFGROW Users	56

List of Acronyms, Abbreviations, and Symbols

a	Crack Length (along the hole bore)
AFGROW	Air Force Crack Growth Life Prediction Software
AFRL	Air Force Research Laboratory
AP/ES, Inc.	Analytical Processes/Engineered Solutions, Incorporated
API	Application Programming Interface
β	Beta Factor (non-dimensional geometry factor used to calculate K)
BCF	Boundary Correction Factor (for pin loading)
c	Crack Length (along the plate width)
COM	Component Object Model (Microsoft Windows)
δ	Displacement
D	Hole Diameter
E	Youngs Modulus
ESRD, Inc.	Engineering Software Research & Development, Inc.
FEM	Finite Element Method
IFF	Interference Fit Fastener
K	Stress Intensity Factor
L	Length
R	Hole Radius
RAM	Random Access Memory
σ	Stress
SIF	Stress Intensity Factor
SMF	Spectrum Multiplication Factor
θ	Lug Loading Angle
T	Plate Thickness
USAF	United States Air Force
ν	Poisson's Ratio
W	Width
Y	Distance (measured from the crack origin along the plate width)
Z	Distance (measured from the crack origin along the hole bore)

List of Figures

Page

Figure 1. Integral Structure Plug-In Schematics Shown with Local Skin Lands at Stiffener	6
Figure 2. Specimen Properties Window for Modified Continuing Damage Plug-In.....	9
Figure 3. Various Crack Front Geometries Inside Integrally Stiffened Fillet Nugget	10
Figure 4. Average Planar Crack Fronts (dashed lines)	11
Figure 5. Lug Geometry and Loading.....	13
Figure 6. Representative StressCheck FEM	14
Figure 7. Effect of W/D on BCF	16
Figure 8. Pin-Lug Load Transfer Idealization.....	24
Figure 9. Lug Geometry, Loads, and Spring Constraints	24
Figure 10. Representative StressCheck Model of Part-through Crack at Loaded Hole in a Lug	25
Figure 11. Load Transfer with a Pin in a Stout Lug.....	29
Figure 12. Lug Model for Fastener	32
Figure 13. Lug Model for Linear Springs Boundary Condition	32
Figure 14. Lug Model for Bearing Stress Load	33
Figure 15. Lug Model Showing Location of Stresses Used for Comparisons	35
Figure 16. Radial Stresses on Lug Hole, $W/D = 1.3$ Fastener is 'neat fit', $\delta/D = 0$	36
Figure 17. (a/b) Normal Stresses from Hole Edge to Lug Edge	38
Figure 18. Radial Stresses on Hole Surface, $\delta/D = 0, 0.0001, 0.001, 0.005, 0.01$	40
Figure 19. Radial Stresses on Hole Surface, $W/D=3$	41
Figure 20. Radial Stresses on Hole Surface, $\delta/D = 0, 0.0001, 0.0005, 0.001$	41
Figure 21. Normal Stresses from Hole Edge to Lug Edge.....	42
Figure 22. Normal Stresses from Hole Edge to Lug Edge for Small Interference	43
Figure 23. Lug Model Loading Configuration and Geometry	46
Figure 24. Lug Loading and Spring Constraints on the Hole Surface. $E_{pin} = 30,000$ ksi; $\nu = 0.3$	46
Figure 25. Stress Intensity Factors Along the Crack Front, $a = 0.95T, 1.1T, 1.5T, 2T$	47
Figure 26. Behavior of β_c as a Crack Transitions from Part-Through to Oblique	49

List of Tables	Page
Table 1. New Geometric Conditions at Pad-Up	8
Table 2. StressCheck Filenames and Applicable Parametric Ranges	14
Table 3. StressCheck Parameter Names and Definitions	15
Table 4. Lug Through Crack Solutions for Bearing and Distributed Spring Loading Conditions	17
Table 5. Range of Parameters for a Lug Part-Through Crack	26
Table 6. Loads and Constraints for Various Lug/Pin Boundary Conditions	29
Table 7. Model Parameter Dimensions	33
Table 8. Parameter Variations in Lug Models	47
Table 9. $K_{I(c)}$ and β_c for Part-Through Cracks Transitioning to Oblique Cracks	49

1. Executive Summary

This is the final report detailing the contractual work performed in the program “Crack Growth and Stress Intensity Prediction Techniques,” which builds upon the efforts of several prior contracts between AP/ES, Anteon, and the United States Air Force.

The challenges of designing modern aircraft continue to drive the development of more advanced analytical tools; often these more advanced analytical tools themselves require development of other enabling technologies such as powerful computers and associated software. The primary historical objective of this project was to develop the infrastructure and to demonstrate that key enabling technologies such as faster and bigger personal computers, as well as database and programming software, have evolved to the point that more advanced analytical tools for analyzing the damage tolerance of aircraft structures are now possible.

Previous contracts successfully established this infrastructure, and contractual work in 2005 was limited to making requested enhancements to several of the computing modules in order to better serve the analytical community.

2. Introduction

2.1 Background

Most damage tolerance analysis tools have not kept pace with advances in computer technology in general. There continues to be a need to analyze structures with complex or unique features – for instance, the types of geometries that may be expected in integral or unitized metallic structures. To date, complex problems have been analyzed using multiple, independent analyses – usually with many simplifying assumptions built-in. This was understandable since the capability to perform more complex and detailed analysis was not available. Recent work performed by the U.S. Air Force Research Laboratory (AFRL) at Wright-Patterson Air Force Base, Ohio, to add a multiple crack analysis capability to (AFGROW) has shown that it is often not feasible to develop closed-form solutions to arbitrary geometries with more than two independent cracks. However, the capability to perform more complex analyses efficiently or even automatically is now within reach due to advances in enabling technologies such as computer software and hardware, and the time is right to move to the next level of complexity in analyses. Experience using the Microsoft component object model (COM) technology has shown that this technology can allow for the integration of a third-party software (called a K-solver in this document) that computes basic fracture mechanics parameters such as Stress Intensity Factors, which will permit real or near real time crack growth life analyses of complex geometries.

This report describes technical efforts, both in 2005 and previously, to develop the next generation life prediction and assessment methods by seamlessly integrating crack growth and finite element method (FEM) K-solver programs. The strategy takes advantage of advances in computing technology to provide direct benefits to the USAF and the aerospace industry. The interaction of a structural FEM code that computes crack tip Mode I stress intensity factors (SIFs) (sometimes referred to as a K-solver or external K-solver) with a crack growth analysis code (such as AFGROW) will provide advanced life assessment and prediction techniques to the structures community. The advanced *p*-version finite element code StressCheck[®] (ESRD, Inc., St. Louis, Missouri, USA) was used for demonstrating the methods and served as a benchmark of the required capability that would be necessary to qualify other possible K-solvers. The StressCheck[®] analysis software is quite capable of fulfilling the computational role, which demands accurate and reliable SIFs, and in addition, is able to efficiently communicate and be controlled with external programming languages via an application programming interface (API), specifically, Microsoft's industry-standard COM. Because the USAF/AFRL crack growth code AFGROW is itself one of the few crack growth codes offering an API (also specifically, Microsoft's COM), StressCheck[®] and AFGROW are jointly very well-suited for interactive programming.

2.2 Previous Work

Recent experience documented in the final report for a previous U.S. AFRL contract¹, has shown that key enabling technologies which will allow the efficient integration of a third party K-solver with widely used crack growth analysis software are now readily available, thereby permitting near real time or real time life analysis of complex geometries. These technologies include

computer hardware that is much more capable (faster speeds, more memory) and affordable than ever before, as well as computer software standards such as the widely available Microsoft COM technology. Some developers' third party K-solvers have used these technologies to improve efficiency and access to their capabilities. One such K-solver that uses the p -version of the finite element code, StressCheck[®] (ESRD, Inc.) has been used to demonstrate integration of a K-solver with the crack growth software AFGROW. ESRD has added COM technology to their code to facilitate integration with AFGROW and other codes, and has worked with quite closely with Analytical Processes/Engineered Solutions (AP/ES) to make this technology work.

The previous project made use of the expertise of individuals who possessed a breadth of knowledge and experience in the enabling technologies. State-of-the-art computational capability for an external K-solver and projections of future computational techniques were obtained from the engineering expertise of ESRD, Inc., the developers of StressCheck[®]. Invaluable descriptions of the internal structure of AFGROW, experience with the user community, and computational needs were provided by Jim Harter of AFRL/VASM and his support personnel. Industry analysts specializing in commercial applications, military transport, fighter, and engine damage tolerance assessments were consulted, along with experts in databases and advanced programming. The experience base also includes developers of fatigue and fracture mechanics methods, procedures, processes, requirements and criteria.

The primary objective of this earlier project was to describe the infrastructure and guidelines to evolve the technology, to plan and prioritize activities, and to ensure the USAF and industry are able to capture the benefits of this technology. The final report described a suggested funding profile that can impact aircraft structural integrity in the near future. The virtually infinite number of structural geometries, loading and cracking configurations were classified into a few problem classes. To aid in setting priorities and evaluating the level of technical skill needed to construct an integrated solution, a complexity rating matrix was presented. For each problem Class, the need for the specific problem solution was documented and an estimate of the Problem Class's complexity and relative priority within the aerospace industry was provided by using a substantiation method which addressed the technical, business and integration cases for the Problem Class. A Solution Strategy or Approach was proposed for each problem class. Due to advances in software technology such as Microsoft COM, it was estimated that Interactive Solution Strategies are presently viable for several Problem Classes, while for other Problem Classes, the current software technology is still not up to speed and would require solutions that would be unwieldy except where often-used internal solutions could be built, and so a Table Look-up Strategy would be more appropriate. For many relatively simple structural geometry and load conditions, a Handbook Strategy would work very well. Finally, for some of the more complex Problem Classes, integrated solutions are simply not feasible or practical at all, at least in the near term.

A system specification with enough detail to allow the integration with AFGROW of any K-solver was described prior to 2004. Requirements for the end integrator of the K-solver and AFGROW product i.e., what the integrator must be capable of, what criteria must be defined, etc. were also defined. Finally, several useful examples of the integration of AFGROW with a K-solver, in this case, ESRD, Inc.'s StressCheck[®], were described.

In 2004, several different integration approaches that linked the AFGROW crack growth analysis

software with an External K-solver were described; the demonstrators for these approaches significantly increased the database of crack growth scenarios that are accessible to the AFGROW user community. These integration approaches included interactive (in which the External K-solver is called by AFGROW only when needed, and automeshing is used extensively), table look up (in which the External K-solver is used to fill in a large database of Geometry Factors β and AFGROW computes Geometry Factors by interpolation and extrapolation of the database), handbook (similar to “interactive”, AFGROW calls the External K-solver only when needed; in contrast to “interactive”, the External K-solver models are developed and checked out *a priori*, and no automeshing is used). AFGROW was previously enhanced to allow externally developed modules to access some necessary routines and functions; this is termed plug in capability. Specific instances of either the interactive integration approach or the handbook integration approach are also referred to as plug ins, as a module for a specific problem type can ‘plug-in’ to AFGROW and effectively supplement the built-in AFGROW stress intensity solution libraries.

The 2004 efforts demonstrated the feasibility of the External K-solver—AFGROW integration approaches on several crack growth scenarios important to current and future aircraft designs. The efforts in particular focused on geometry and solutions that are important for integral structure applications that are being pursued for designs offering cost advantages due to manufacturing options. Many challenges were successfully overcome, thanks to evolving ancillary technologies such as computing horsepower and advances in programming and communications software. While many industry useful crack growth scenarios (including integral structures, notches, and lugs) have been added as ‘plug-ins’ to the AFGROW crack growth software, many more just as useful scenarios can be easily added to make AFGROW even more beneficial to the industry and to military customers. It is clear that the potential of this technology and the demonstrated integration approaches has only begun to be tapped by the military and the aircraft industry. The solutions provided to date offer the industry accurate advances in assessment methods that have not been available or where solution accuracy was either poor or questionable.

2.3 2005 Original Scope

The original statement of work called for the completion of 3 Technical Tasks: Integral Structure Plug-in Modifications, Methods Development and FE Modeling for Interference Fit Fasteners (IFF), and Software Modifications and Development. Key capabilities were to be added to the Integral Structure models that were developed and tested in 2004 through the use of ‘plug-ins’ that could seamlessly integrate with the existing AFGROW-External K-solver interface: continuing damage plug in with pad-ups, and enhanced two-bay crack plug in with pad-ups (pad-ups are small substructures at the bottom of the stiffeners in the integral structures—in a cutaway view, with the plate and stiffeners in cross section of the crack plane, the pad-ups look like small spacers that are located between the stiffeners and the plate. The entire structure is still cut from one block of material).

The Methods Development and FE Modeling for IFF and Software Modifications and Development tasks required the development, checkout and delivery of an integrated AFGROW-External K-solver that could model Interference Fit Fasteners. StressCheck® (ESRD, Inc., St. Louis, MO) again was designated the External K-solver in the task; however, the capability to

adequately model IFFs did not exist prior to 2005, requiring that we wait until the capability was developed by ESRD before putting together the AFGROW-External K-solver integration. As of August 2005, the IFF capability was not yet available in StressCheck, therefore at the customer's request, this task was rescoped and described in the next section.

2.4 2005 Revised Scope

The Methods Development and Software Modifications tasks described in the previous section were modified in August 2005 when it became apparent the enabling modifications to StressCheck were not going to be made in time to complete the two tasks; therefore, these tasks were changed (with the approval of the primary USAF customer and the OEM customer) to the yield the following deliverables:

1. Rerun all previously tabulated 3-D lug cases using distributed spring loading conditions or contact loading conditions.
2. Create tabular lookup solutions for 2-D lugs using a cosine bearing load distribution—this expanded existing AFGROW 2-D solutions which used distributed spring loading conditions.
3. Compare cracked-plane stress profiles for 2-D lugs: (a) cosine bearing stress results, (b) distributed spring stress results, and (c) StressCheck stress results for various levels of interference fit. These comparisons should provide information on which, if either, loading condition best represents light levels of interference (i.e., press-fit bushings or similar features).
4. Provide 3-D Mode I Stress Intensity Factors (SIFs) K_I , along lug crack fronts for correlation with mechanical lug marker band tests at Purdue University.

2.5 Participants

The primary customer for this contract is the U.S. Air Force Research Laboratories at Wright-Patterson Air Force Base in Dayton, Ohio, which is the developer of the crack growth analysis computer software AFGROW. The work performed by APES under this effort is directly applicable to enhancing that AFRL software, as well as advancing the state-of-the-art for crack growth and damage tolerance predictions in the aerospace and other commercial industries. In 2004 and 2005, the Anteon Corporation served as the direct contractor to the USAF, provided the experience and contractual expertise required for dealing with the USAF APES, Incorporated served as the primary technical lead on this contract. LexTech, Inc. provided the ability to modify and release the AFGROW code in support of the contractual goals. The Boeing Company provided technical advice, a link to aircraft field problems, some components of the technical effort, checkout and evaluation of the plug-ins, and arranged the mechanical test effort. Purdue University provided the mechanical test support for this program through Boeing.

2.6 Report Outline

The rest of the report is organized as follows: the two AFGROW-External K-solver plug-in enhancements are described in Section 3, results for the 2-D Lug Finite Element Solutions with the Cosine Bearing Load are found in Section 4, 3-D Lug Finite Element Solutions with the Distributed Spring boundary conditions are described in Section 5, the Lug Boundary Condition Effects are found in Section 6, and Support for Purdue Experimental Lug Tests is described in Section 7.

3. AFGROW External K-Solver: Integral Structure Plug-in Modifications

3.1 Objective and Description

In 2004, two plug-ins using the ‘interactive’ integration approach were developed. The two plug-ins were similar, and both addressed integrally stiffened structure: one for a continuing damage crack at the edge of a fastener hole, and the other for a centrally cracked stiffener in an integrally stiffened panel (used to evaluate the traditional damage tolerance criteria of a two-bay crack). Based on feedback from the OEM customer, both of these plug-ins were enhanced in 2005 to allow “pad-ups”, or “lands”, at the central stiffener. The pad-up parametric geometry specification allows either a traditionally shaped slightly thicker skin near the stiffener (as in built-up chemically milled skin structure), or a large, more squarish mass of material around the stiffener that acts more like a crenellation. Additionally, several limitations on the crack front shape were addressed, as well as assumptions of the crack shapes during automated propagation of the crack. Finally, enforced displacements were implemented as a loading option for the integral structure plug-ins.

3.2 Integral Structure--Modifications to Plug-Ins

Both the continuing damage integral structure plug-in model (Figure 1, left) and the two-bay crack integral structure plug-in model (Figure 1, right) were modified to include the additional parametric variables Wl and Tl (width of land and thickness of land) as shown in the figure.

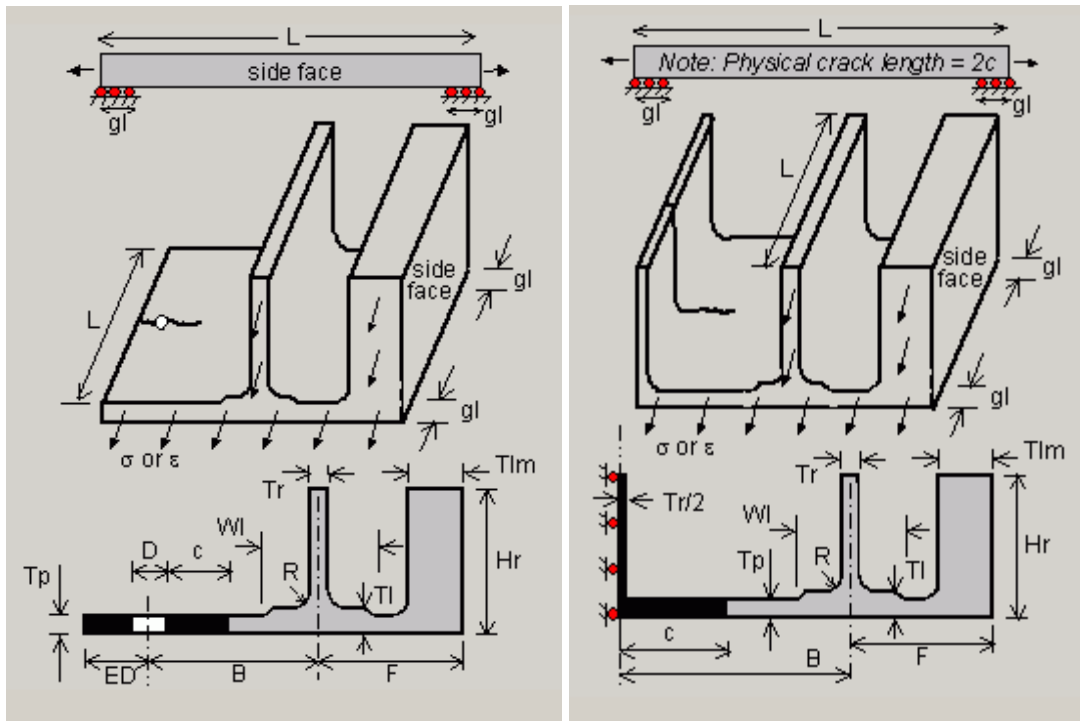
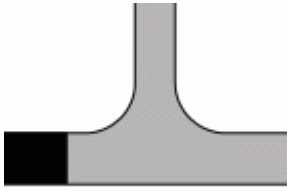
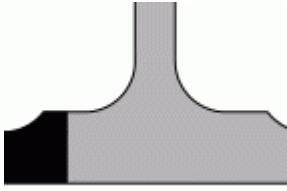
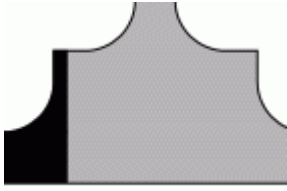
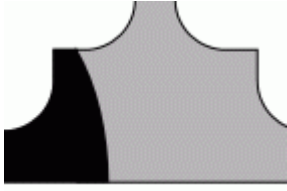


Figure 1. Integral Structure Plug-In Schematics Shown with Local Skin Lands at Stiffener

The radius R is kept constant throughout the part, as numerically-controlled machining of these types of parts would nearly always use a constant fillet radius on the cutting bit. The addition of the pad-ups presents three geometric cases that are all accounted for within the plug-in code. Table 1 shows these three cases, A, B, and C. In all three cases, the crack front remains straight and vertical whether it is in the skin, in the radius leading to the land, or in the land itself. Once the crack length is long enough such that the crack front is located to the *right* of the radius tangency leading to the *stiffener* (case D), the crack front definition makes use of the other two crack parameters, a and lc . Case D then presents other complications due to the many possible intersection locations of the upper part of the crack front. However, they are handled sufficiently by the computer code and will not be discussed here.

Table 1. New Geometric Conditions at Pad-Up

Geometric Condition	Description	Picture
(A) $Tl = Tp$	No pad-up	
(B) $Tl - Tp < R$	Partial radius into pad-up	
(C) $Tl - Tp \geq R$	Full radius into pad-up	
(D) Crack front c right of stiffener-land fillet tangency	Curved crack front definition is used (crack front parameters a and lc become active)	

In addition to the pad-up functionality, enforced displacement is now an option instead of an applied stress loading. Figure 2 shows the AFGROW Specimen Properties plug-in window for the continuing damage model, the “Load Type” entry is now a pull-down selection of either “Stress” or “Displacement”. If “Stress” is selected, the standard AFGROW means of computing the reference stress σ is used (the Spectrum Multiplication Factor, SMF, multiplied by the current AFGROW spectrum stress level). If “Displacement” is selected, a fixed displacement will be applied to the finite-element model of the component, with the displacement δ calculated as:

$$\delta = \frac{\sigma}{E} \left(\frac{L}{2} \right) \quad (1)$$

The enforced displacement solution is useful to help bracket the true stress intensity solution. In correlation with cracked integral structure experiments conducted in 2004 and 2005 [2], the stress intensity factors due to applied stress and the values due to applied displacement generally

fell above and below the experimental values, respectively.

Item	Value
(Name)	Continuing Damage in an Inte...
Edge Distance ED	0.5
Hole Diameter D	0.25
Stiffener Location B	2.66
Overhang F	4.1
Plate Thickness T _p	0.25
Fillet Radius R	0.25
Stiffener Thickness T _r	0.2
Stiffener Height H _r	3
Panel Length L	22.2
Crack Length c	0.375
Local Crack Length l _c	0.5
Crack Length a	0.5
Lumped Mass Thickness T _{lm}	1
Lumped Mass Height H _{lm}	3
Stiffener Land Width W _l	3
Stiffener Land Thickness T _l	0.4
Load Type	Stress
Grip Length g _l	1.5
Modulus	450000
Nu	0.3
Min p-level	1
Max p-level	1

Figure 2. Specimen Properties Window for Modified Continuing Damage Plug-In

3.3 Enhancements

During the contracted modification procedure, other issues were addressed in an attempt to better model the physical crack front propagation through an integral stiffener. Previously, as a crack such as Figure 3(a) grew and passed the geometrically-limiting case of Figure 3(b), a transition would occur where the curved crack front instantaneously transitioned to two planar crack fronts just (0.03 inch) *outside* each fillet tangency (known as crack stage 6). This gross assumption did not take into account the crack shape or size before transition. New capability has been added so that planar (straight) cracks fronts (crack stage 5.5) are now allowed *within* the stiffener fillet radius, such as shown in Figure 3(c) and 3(d). This improves the accuracy of the transition to two through cracks as the single part-through crack progresses through the stiffener. The skin and stiffener intersection points of the transitional curved crack in Figure 3(b) are used to compute average planar crack positions just after transition, Figure 4. The intersection points are indicated by arrows in Figure 4. Note that two planar cracks, *both* within their respective fillet

radii, cannot be specified as a starting condition by the user; this condition can only be achieved through automated crack propagation by the computer code. Figure 3(c) or 3(d) can be specified as a starting condition, but not the combination of 3(c) and 3(d).

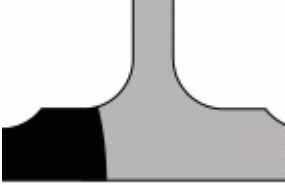
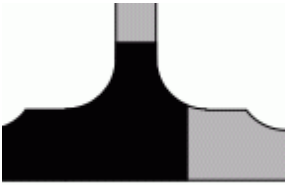
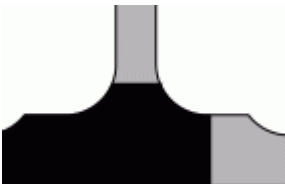
Description	Picture
(a) Crack Stage 5 (curved crack front definition)	
(b) Crack Stage 5, near transition to Crack Stage 6 (transition occurs when crack front mesh intersects exit-side fillet)	
(c) Crack Stage 5.5 after transition. New capability of skin crack within fillet tangencies is displayed	
(d) Crack stage 5.5 showing new capability of stiffener crack front inside fillet tangencies	

Figure 3. Various Crack Front Geometries Inside Integrally Stiffened Fillet Nugget

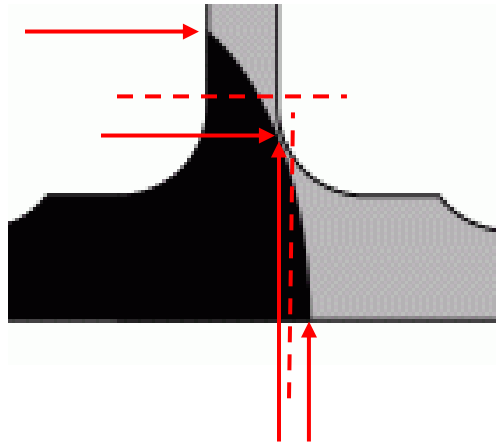


Figure 4. Average Planar Crack Fronts (dashed lines)

3.4 Challenges

Most of the challenges that arose during 2004 development of the two integral structure plug-ins have been resolved. The primary challenge was the version inconsistencies in COM function calls to StressCheck and AFGROW during development. This meant that as one software component's version was updated to address a bug, sections of the code that were previously working would cease to operate properly. However, in 2005, stable versions of StressCheck, AFGROW, and the plug-in components were all released and operating successfully together. The Boeing Company (Huntington Beach), under separate contract, evaluated plug-in operation and functionality, and made use of these stable versions of the various computer codes.

3.5 Limitations

PC processing speed continues to be an issue with the computationally-intensive 3-D finite element solutions used to extract the stress intensity factor for each incremental step during a crack growth analysis. An analysis in which the crack length advances several inches and a sufficiently converged stress intensity solution is computed with every 5 percent change in the crack length may take several hours to run on a state-of-the-art consumer PC. However, as processor speed continues to increase and RAM continues to become more affordable, the elapsed time required to complete an analysis will decrease.

3.6 Conclusions and Recommendations

The option of using pad-ups around the integral stiffener in these two plug-in modules will allow a wider variety of integral structures to be examined for damage tolerance, and allows new configurations to be considered during trade studies. The enhanced features can allow a better understanding of crack propagation modes and mechanisms in integral structure, and can hopefully provide insights into the establishment of new design criteria and guidelines for integral structure, so that structural safety can be maintained or enhanced while the cost and assembly benefits of using integral structure in place of built-up structure can be realized.

4. 2-D Lug Finite Element Solutions: Cosine Bearing Load

4.1 Objective

The objective of this study was to compute a matrix of accurate and reliable Mode I Stress Intensity Factors for a Two-Dimensional lug with a single through crack in the case of the pin load transfer being modeled as a cosine bearing traction on the lug hole. These solutions supplement the existing AFGROW database of 2-D lug solutions that use an unknown and perhaps different method of modeling the pin load transfer.

4.2 Approach

Lugs can be found in many different substructures in an aircraft: wing attach fittings and control linkages among others. AFGROW currently contains a 2-D model for a single Through Crack in a Lug. However, users of this AFGROW crack growth model in the past have indicated that the results from the AFGROW analyses can be suspect; therefore, adding to the expanded lug solutions was a major goal of this project.

The load transfer between a pin (neat-fit) and a stout lug was modeled with the finite element method, Figure 5. The *p*-version finite element method software StressCheck[®] (ESRD, St. Louis, MO) was used to simulate the interaction of a lug with a load transfer pin; the goal of the analyses was to provide tabulated values of accurate and reliable Mode I Stress Intensity Factors (SIFs) for a 2-D Through Crack in a Lug for eventual incorporation into existing AFGROW databases. All finite element models are two-dimensional models subjected to a bearing stress (or traction) $\sigma_b = A \cos(\theta)$, Equation (2). The results from these models are designed to round out the existing AFGROW database of 3-D lug solutions that used this cosine bearing function to model the pin-lug load transfer.

$$\sigma_b = A \cos(\theta) = \frac{4P}{\pi Dt} \cos(\theta) \quad (2)$$

where: P is the simulate pin load (that is, the net force on the lug hole),

D is the hole diameter,

t is the lug thickness, and

θ is the angle with respect to the horizontal.

4.3 Schematic

Two-Dimensional plane stress finite element models of single through cracks at a hole in a lug were modeled with StressCheck[®]. The pin-lug load transfer was modeled with a distributed bearing stress defined by Equation (2); Figure 5 below is a schematic and model load and constraints of the lug. A typical StressCheck finite element model is shown in Figure 6.

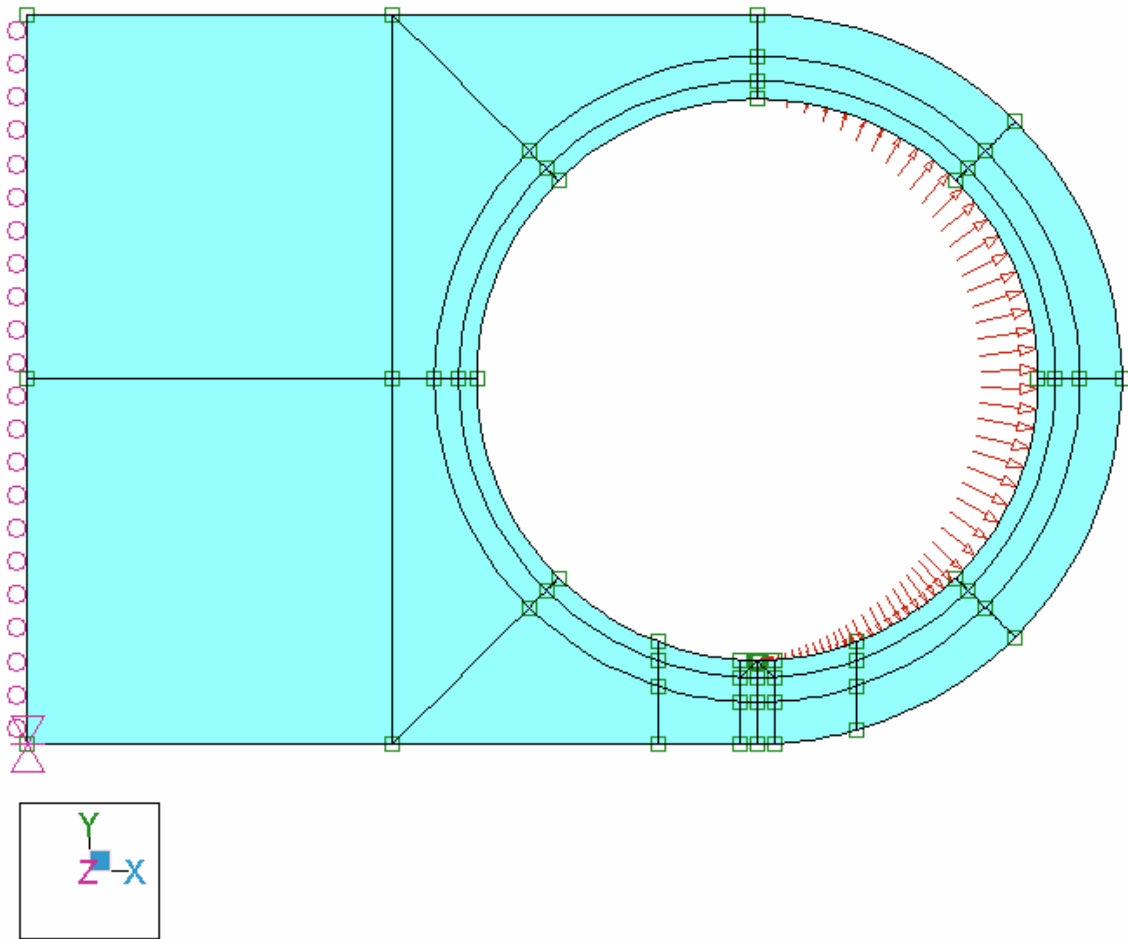


Figure 5. Lug Geometry and Loading

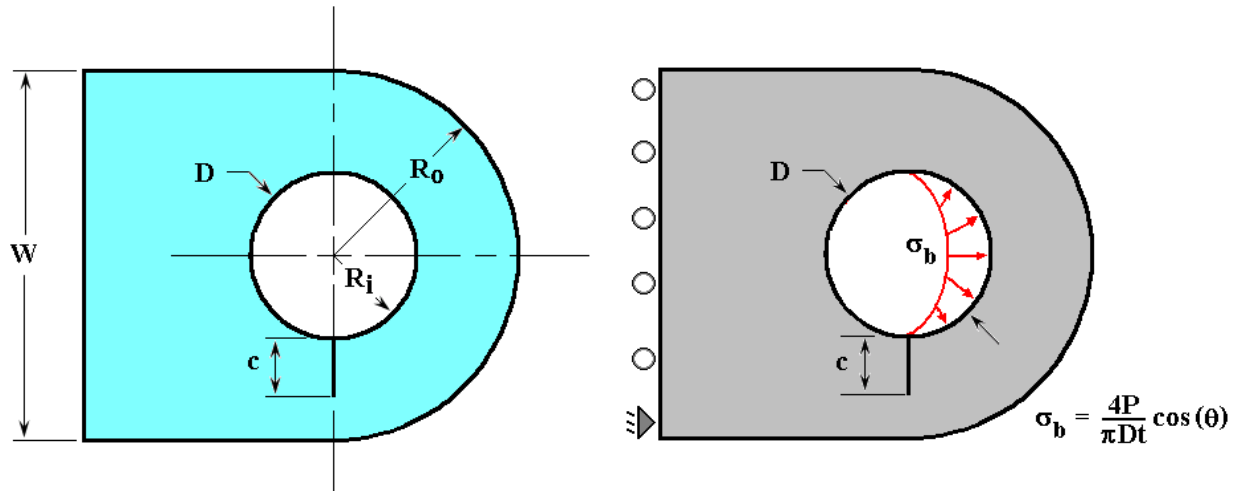


Figure 6. Representative StressCheck FEM

4.4 Results

The StressCheck input file names (*.SCI) and range of parameters for which these *.SCI files are valid are listed in Table 2. Note the diameter parameter name D is referred to as Dh in the StressCheck parameter list.

Table 2. StressCheck Filenames and Applicable Parametric Ranges

Crack Ratio $c/(R_o - R_i)$	Width/Diameter W/D	*.sci File Name
$0.005 \leq c/(R_o - R_i) \leq 0.05$	$1.3 \leq W/D \leq 2.0$	2-Dlug1a2.sci
$0.005 \leq c/(R_o - R_i) \leq 0.10$	$2.5 \leq W/D \leq 5.0$	2-Dlug1a2.sci
$0.1 \leq c/(R_o - R_i) \leq 0.3$	$1.3 \leq W/D \leq 2.0$	2-Dlug2.sci
$0.1 \leq c/(R_o - R_i) \leq 0.3$	$2.5 \leq W/D \leq 5.0$	2-Dlug2a.sci
$0.35 \leq c/(R_o - R_i) \leq 0.95$	$1.3 \leq W/D \leq 2.0$	2-Dlug3.sci
$0.35 \leq c/(R_o - R_i) \leq 0.95$	$2.5 \leq W/D \leq 5.0$	2-Dlug4.sci

Table 3 below lists the parameter names as defined in the family of StressCheck input (*.sci) files. All length dimensions are in inches.

Table 3. StressCheck Parameter Names and Definitions

*.sci Parameter Name	*.s ci Pa ra me ter De scr ipt io n	Detail Description
awd	W/D	Width-Diameter ratio; model construction parameter.
c	crack length	Crack length.
Dh	Diameter (D)	Hole diameter.
dim	dimension	Model construction parameter.
Epin	Pin Modulus	Modulus of Elasticity of the bearing.
Fpin	Pin force	Force input parameter, defined as $Dh \cdot th$ to produce a bearing stress of 1 ksi.
Kn	Spring Coefficient	Spring constraint coefficient, defined as $2 \cdot E_{pin} / (Dh \cdot (1 + \nu)(1 - 2 \cdot \nu))$, where $\nu = 0.3$.
L	length	Model length as measured from the center of the lug hole. Fixed at $L = W = 2 \cdot Ro$.
po	point offset (deg)	Model construction parameter used for crack mesh construction.
Ri	Hole Radius	$0.5 \cdot Dh$
Ro	Lug Outer Radius	Lug Outer Radius.
St	stress	Applied stress. Defined as Dh/L to produce a bearing stress of 1 ksi.
th	thickness	Model thickness, defined as 1.

Parametric values spanning a range of W/D from $1.3 \leq W/D \leq 5.0$ were selected for a fixed diameter $D = 0.50$. Table 4 below shows the boundary correction factors (BCFs), β compiled for the lookup tables. The Boundary Correction Factors for the distributed spring constraint are also tabulated here for comparison. The effect of W/D on the Boundary Correction Factors (BCFs) from minimum to maximum length for a given W/D is found in Figure 7 below. It is evident that the differences in the BCFs between the models used to model the pin-lug load transfer, bearing stress and normal spring constraints, become less and less as the W/D increases, becoming negligible for $W/D = 5.0$.

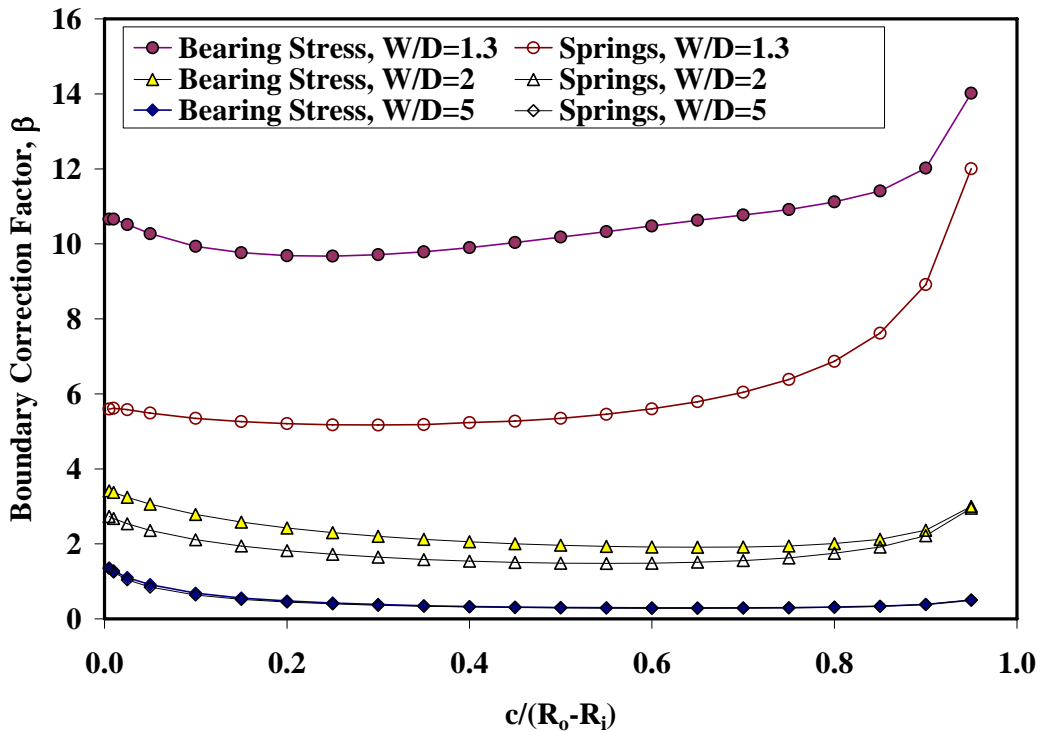


Figure 7. Effect of W/D on BCF

Table 4. Lug Through Crack Solutions for Bearing and Distributed Spring Loading Conditions

*.sci	Crack Ratio	Diameter	Crack			Bearing		Spring	
Filename	$c/(R_o - R_i)$	D , in.	C , in.	$R_o - R_i$	W/D	K_I	β_b	K_I	β_s
2-DLug1a2	0.005	0.5	0.000375	0.075	1.3	0.3658	10.6573	0.192	5.594
2-DLug1a2	0.01	0.5	0.00075	0.075	1.3	0.5173	10.6581	0.2725	5.615
2-DLug1a2	0.025	0.5	0.001875	0.075	1.3	0.8068	10.5125	0.4279	5.576
2-DLug1a2	0.05	0.5	0.00375	0.075	1.3	1.1147	10.2701	0.5955	5.486
2-DLug2	0.1	0.5	0.0075	0.075	1.3	1.5246	9.9321	0.8205	5.346
2-DLug2	0.15	0.5	0.01125	0.075	1.3	1.8352	9.7617	0.9891	5.261
2-DLug2	0.2	0.5	0.015	0.075	1.3	2.1017	9.6815	1.1301	5.206
2-DLug2	0.25	0.5	0.01875	0.075	1.3	2.3472	9.6709	1.2561	5.176
2-DLug2	0.3	0.5	0.0225	0.075	1.3	2.5822	9.7122	1.3735	5.166
2-DLug3	0.35	0.5	0.02625	0.075	1.3	2.8095	9.7834	1.4878	5.181
2-DLug3	0.4	0.5	0.03	0.075	1.3	3.039	9.8992	1.6058	5.231
2-DLug3	0.45	0.5	0.03375	0.075	1.3	3.2668	10.0324	1.7154	5.268
2-DLug3	0.5	0.5	0.0375	0.075	1.3	3.4931	10.1769	1.8354	5.347
2-DLug3	0.55	0.5	0.04125	0.075	1.3	3.7176	10.3271	1.9641	5.456
2-DLug3	0.6	0.5	0.045	0.075	1.3	3.9397	10.4782	2.1048	5.598
2-DLug3	0.65	0.5	0.04875	0.075	1.3	4.1583	10.6257	2.2658	5.79
2-DLug3	0.7	0.5	0.0525	0.075	1.3	4.3732	10.7683	2.4532	6.04
2-DLug3	0.75	0.5	0.05625	0.075	1.3	4.5875	10.913	2.6833	6.383
2-DLug3	0.8	0.5	0.06	0.075	1.3	4.8276	11.1194	2.9824	6.869
2-DLug3	0.85	0.5	0.06375	0.075	1.3	5.1055	11.4084	3.409	7.617
2-DLug3	0.9	0.5	0.0675	0.075	1.3	5.5335	12.0163	4.1035	8.911
2-DLug3	0.95	0.5	0.07125	0.075	1.3	6.6295	14.0124	5.6798	12.005
2-DLug1a2	0.005	0.5	0.0005	0.1	1.4	0.3227	8.1415	0.187	4.719
2-DLug1a2	0.01	0.5	0.001	0.1	1.4	0.4554	8.1254	0.2643	4.715
2-DLug1a2	0.025	0.5	0.0025	0.1	1.4	0.7073	7.9809	0.4113	4.641
2-DLug1a2	0.05	0.5	0.005	0.1	1.4	0.9722	7.7571	0.5663	4.518
2-DLug2	0.1	0.5	0.01	0.1	1.4	1.318	7.4359	0.7678	4.332
2-DLug2	0.15	0.5	0.015	0.1	1.4	1.57	7.2322	0.912	4.201
2-DLug2	0.2	0.5	0.02	0.1	1.4	1.7798	7.1005	1.029	4.105
2-DLug2	0.25	0.5	0.025	0.1	1.4	1.9673	7.0198	1.1311	4.036
2-DLug2	0.3	0.5	0.03	0.1	1.4	2.1415	6.9757	1.2245	3.989
2-DLug3	0.35	0.5	0.035	0.1	1.4	2.3057	6.9533	1.1637	3.509
2-DLug3	0.4	0.5	0.04	0.1	1.4	2.4669	6.959	1.255	3.54
2-DLug3	0.45	0.5	0.045	0.1	1.4	2.6237	6.9779	1.3481	3.585
2-DLug3	0.5	0.5	0.05	0.1	1.4	2.7769	7.0065	1.4463	3.649

2-DLug3	0.55	0.5	0.055	0.1	1.4	2.9272	7.0419	1.553	3.736
2-DLug3	0.6	0.5	0.06	0.1	1.4	3.0752	7.0831	1.6722	3.852
2-DLug3	0.65	0.5	0.065	0.1	1.4	3.2221	7.1303	1.8095	4.004
2-DLug3	0.7	0.5	0.07	0.1	1.4	3.3703	7.187	1.9723	4.206
2-DLug3	0.75	0.5	0.075	0.1	1.4	3.5259	7.2638	2.1733	4.477
2-DLug3	0.8	0.5	0.08	0.1	1.4	3.711	7.4024	2.4998	4.986
2-DLug3	0.85	0.5	0.085	0.1	1.4	3.9468	7.6378	2.8498	5.515
2-DLug3	0.9	0.5	0.09	0.1	1.4	4.3368	8.156	3.4281	6.447
2-DLug3	0.95	0.5	0.095	0.1	1.4	5.3228	9.7433	4.7286	8.656
2-DLug1a2	0.005	0.5	0.000625	0.125	1.5	0.2907	6.5601	0.1829	4.128
2-DLug1a2	0.01	0.5	0.00125	0.125	1.5	0.4096	6.5357	0.2575	4.11
2-DLug1a2	0.025	0.5	0.003125	0.125	1.5	0.6336	6.3947	0.3976	4.013
2-DLug1a2	0.05	0.5	0.00625	0.125	1.5	0.8667	6.1851	0.5424	3.871
2-DLug2	0.1	0.5	0.0125	0.125	1.5	1.1645	5.8762	0.7252	3.66
2-DLug2	0.15	0.5	0.01875	0.125	1.5	1.3745	5.6635	0.8514	3.508
2-DLug2	0.2	0.5	0.025	0.125	1.5	1.5446	5.5116	0.9511	3.394
2-DLug2	0.25	0.5	0.03125	0.125	1.5	1.6925	5.4016	1.0363	3.307
2-DLug2	0.3	0.5	0.0375	0.125	1.5	1.8266	5.3217	1.1133	3.243
2-DLug3	0.35	0.5	0.04375	0.125	1.5	1.9504	5.2608	1.1044	2.979
2-DLug3	0.4	0.5	0.05	0.125	1.5	2.0696	5.2218	1.1766	2.969
2-DLug3	0.45	0.5	0.05625	0.125	1.5	2.1841	5.1955	1.2499	2.973
2-DLug3	0.5	0.5	0.0625	0.125	1.5	2.2951	5.1796	1.3273	2.995
2-DLug3	0.55	0.5	0.06875	0.125	1.5	2.404	5.1728	1.412	3.038
2-DLug3	0.6	0.5	0.075	0.125	1.5	2.512	5.175	1.5076	3.106
2-DLug3	0.65	0.5	0.08125	0.125	1.5	2.6211	5.188	1.6189	3.204
2-DLug3	0.7	0.5	0.0875	0.125	1.5	2.7348	5.2162	1.7525	3.343
2-DLug3	0.75	0.5	0.09375	0.125	1.5	2.8599	5.2697	1.9195	3.537
2-DLug3	0.8	0.5	0.1	0.125	1.5	3.0159	5.3807	2.1913	3.91
2-DLug3	0.85	0.5	0.10625	0.125	1.5	3.2257	5.5833	2.4887	4.308
2-DLug3	0.9	0.5	0.1125	0.125	1.5	3.5836	6.0279	2.986	5.023
2-DLug3	0.95	0.5	0.11875	0.125	1.5	4.4771	7.3301	4.1108	6.73
2-DLug1a2	0.005	0.5	0.000938	0.1875	1.75	0.2409	4.4396	0.1756	3.236
2-DLug1a2	0.01	0.5	0.001875	0.1875	1.75	0.338	4.4045	0.2453	3.196
2-DLug1a2	0.025	0.5	0.004688	0.1875	1.75	0.5183	4.2707	0.3723	3.068
2-DLug1a2	0.05	0.5	0.009375	0.1875	1.75	0.7002	4.0802	0.4979	2.901
2-DLug2	0.1	0.5	0.01875	0.1875	1.75	0.9203	3.7921	0.6466	2.664
2-DLug2	0.15	0.5	0.028125	0.1875	1.75	1.0645	3.5812	0.7418	2.496
2-DLug2	0.2	0.5	0.0375	0.1875	1.75	1.1738	3.4197	0.8131	2.369
2-DLug2	0.25	0.5	0.046875	0.1875	1.75	1.2634	3.2923	0.8716	2.271
2-DLug2	0.3	0.5	0.05625	0.1875	1.75	1.341	3.1899	0.9232	2.196
2-DLug3	0.35	0.5	0.065625	0.1875	1.75	1.4102	3.1057	0.9506	2.094

2-DLug3	0.4	0.5	0.075	0.1875	1.75	1.4751	3.0389	0.9962	2.052
2-DLug3	0.45	0.5	0.084375	0.1875	1.75	1.5369	2.9852	1.0427	2.025
2-DLug3	0.5	0.5	0.09375	0.1875	1.75	1.5973	2.9432	1.0926	2.013
2-DLug3	0.55	0.5	0.103125	0.1875	1.75	1.6577	2.9124	1.1483	2.017
2-DLug3	0.6	0.5	0.1125	0.1875	1.75	1.72	2.8933	1.2126	2.04
2-DLug3	0.65	0.5	0.121875	0.1875	1.75	1.7866	2.8873	1.2892	2.083
2-DLug3	0.7	0.5	0.13125	0.1875	1.75	1.8611	2.8984	1.3829	2.154
2-DLug3	0.75	0.5	0.140625	0.1875	1.75	1.95	2.9338	1.5023	2.26
2-DLug3	0.8	0.5	0.15	0.1875	1.75	2.0685	3.0132	1.6906	2.463
2-DLug3	0.85	0.5	0.159375	0.1875	1.75	2.238	3.1628	1.9107	2.7
2-DLug3	0.9	0.5	0.16875	0.1875	1.75	2.5337	3.4798	2.2837	3.137
2-DLug3	0.95	0.5	0.178125	0.1875	1.75	3.2552	4.3515	3.1326	4.188
2-DLug1a2	0.005	0.5	0.00125	0.25	2	0.2139	3.4128	0.1712	2.732
2-DLug1a2	0.01	0.5	0.0025	0.25	2	0.2988	3.3719	0.2373	2.678
2-DLug1a2	0.025	0.5	0.00625	0.25	2	0.4541	3.2405	0.355	2.533
2-DLug1a2	0.05	0.5	0.0125	0.25	2	0.6059	3.0574	0.4667	2.355
2-DLug2	0.1	0.5	0.025	0.25	2	0.7795	2.7813	0.5915	2.111
2-DLug2	0.15	0.5	0.0375	0.25	2	0.8851	2.5788	0.6665	1.942
2-DLug2	0.2	0.5	0.05	0.25	2	0.9604	2.4231	0.7199	1.816
2-DLug2	0.25	0.5	0.0625	0.25	2	1.0191	2.3	0.7625	1.721
2-DLug2	0.3	0.5	0.075	0.25	2	1.0683	2.2008	0.7994	1.647
2-DLug3	0.35	0.5	0.0875	0.25	2	1.1114	2.1198	0.8284	1.58
2-DLug3	0.4	0.5	0.1	0.25	2	1.1518	2.0549	0.8603	1.535
2-DLug3	0.45	0.5	0.1125	0.25	2	1.1907	2.0029	0.8935	1.503
2-DLug3	0.5	0.5	0.125	0.25	2	1.2297	1.9623	0.9298	1.484
2-DLug3	0.55	0.5	0.1375	0.25	2	1.2702	1.9325	0.9713	1.478
2-DLug3	0.6	0.5	0.15	0.25	2	1.3138	1.9138	1.02	1.486
2-DLug3	0.65	0.5	0.1625	0.25	2	1.3626	1.9071	1.0788	1.51
2-DLug3	0.7	0.5	0.175	0.25	2	1.4201	1.9153	1.1517	1.553
2-DLug3	0.75	0.5	0.1875	0.25	2	1.4918	1.9437	1.2454	1.623
2-DLug3	0.8	0.5	0.2	0.25	2	1.5901	2.006	1.3872	1.75
2-DLug3	0.85	0.5	0.2125	0.25	2	1.734	2.1222	1.5639	1.914
2-DLug3	0.9	0.5	0.225	0.25	2	1.9857	2.3619	1.8647	2.218
2-DLug3	0.95	0.5	0.2375	0.25	2	2.5908	2.9993	2.5504	2.953
2-DLug1a2	0.005	0.5	0.001875	0.375	2.5	0.1875	2.4431	0.1668	2.174
2-DLug1a2	0.01	0.5	0.00375	0.375	2.5	0.2599	2.3949	0.2282	2.103
2-DLug1a2	0.025	0.5	0.009375	0.375	2.5	0.3879	2.2604	0.3327	1.939
2-DLug2a	0.05	0.5	0.01875	0.375	2.5	0.5043	2.0779	0.4244	1.749
2-DLug2a	0.1	0.5	0.0375	0.375	2.5	0.6235	1.8165	0.5169	1.506
2-DLug3	0.15	0.5	0.05625	0.375	2.5	0.681	1.62	0.5572	1.326
2-DLug3	0.2	0.5	0.075	0.375	2.5	0.7228	1.4891	0.5968	1.23

2-DLug3	0.25	0.5	0.09375	0.375	2.5	0.7518	1.3852	0.6229	1.148
2-DLug3	0.3	0.5	0.1125	0.375	2.5	0.7746	1.3029	0.643	1.082
2-DLug4	0.35	0.5	0.13125	0.375	2.5	0.7937	1.236	0.6602	1.028
2-DLug4	0.4	0.5	0.15	0.375	2.5	0.8135	1.185	0.6805	0.991
2-DLug4	0.45	0.5	0.16875	0.375	2.5	0.8336	1.1449	0.7022	0.964
2-DLug4	0.5	0.5	0.1875	0.375	2.5	0.8552	1.1143	0.7265	0.947
2-DLug4	0.55	0.5	0.20625	0.375	2.5	0.8793	1.0923	0.7545	0.937
2-DLug4	0.6	0.5	0.225	0.375	2.5	0.9071	1.0789	0.7876	0.937
2-DLug4	0.65	0.5	0.24375	0.375	2.5	0.9404	1.0746	0.8279	0.946
2-DLug4	0.7	0.5	0.2625	0.375	2.5	0.9816	1.0809	0.8783	0.967
2-DLug4	0.75	0.5	0.28125	0.375	2.5	1.0351	1.1012	0.9436	1.004
2-DLug4	0.8	0.5	0.3	0.375	2.5	1.1115	1.145	1.035	1.066
2-DLug4	0.85	0.5	0.31875	0.375	2.5	1.2239	1.223	1.1675	1.167
2-DLug4	0.9	0.5	0.3375	0.375	2.5	1.4172	1.3763	1.3886	1.348
2-DLug4	0.95	0.5	0.35625	0.375	2.5	1.8709	1.7685	1.8863	1.783
2-DLug1a2	0.005	0.5	0.0025	0.5	3	0.1763	1.9893	0.1655	1.868
2-DLug1a2	0.01	0.5	0.005	0.5	3	0.2426	1.9355	0.2238	1.786
2-DLug2a	0.025	0.5	0.0125	0.5	3	0.3537	1.7849	0.3173	1.601
2-DLug2a	0.05	0.5	0.025	0.5	3	0.4512	1.6101	0.3967	1.415
2-DLug2a	0.1	0.5	0.05	0.5	3	0.5373	1.3558	0.4667	1.177
2-DLug2a	0.15	0.5	0.075	0.5	3	0.5751	1.1847	0.4988	1.028
2-DLug3	0.2	0.5	0.1	0.5	3	0.5942	1.0602	0.5178	0.924
2-DLug3	0.25	0.5	0.125	0.5	3	0.6084	0.9709	0.5324	0.85
2-DLug3	0.3	0.5	0.15	0.5	3	0.6194	0.9023	0.5435	0.792
2-DLug3	0.35	0.5	0.175	0.5	3	0.6297	0.8493	0.5541	0.747
2-DLug3	0.4	0.5	0.2	0.5	3	0.6406	0.8082	0.5658	0.714
2-DLug3	0.45	0.5	0.225	0.5	3	0.6529	0.7766	0.5796	0.689
2-DLug3	0.5	0.5	0.25	0.5	3	0.6673	0.7529	0.5962	0.673
2-DLug3	0.55	0.5	0.275	0.5	3	0.6844	0.7363	0.6165	0.663
2-DLug3	0.6	0.5	0.3	0.5	3	0.7052	0.7264	0.6415	0.661
2-DLug3	0.65	0.5	0.325	0.5	3	0.7309	0.7233	0.6725	0.665
2-DLug3	0.7	0.5	0.35	0.5	3	0.7637	0.7283	0.7116	0.679
2-DLug3	0.75	0.5	0.375	0.5	3	0.8069	0.7435	0.7627	0.703
2-DLug3	0.8	0.5	0.4	0.5	3	0.8682	0.7745	0.8315	0.742
2-DLug3	0.85	0.5	0.425	0.5	3	0.9596	0.8305	0.9334	0.808
2-DLug3	0.9	0.5	0.45	0.5	3	1.1185	0.9407	1.1072	0.931
2-DLug3	0.95	0.5	0.475	0.5	3	1.4897	1.2194	1.5024	1.23
2-DLug1a2	0.005	0.5	0.003438	0.6875	3.75	0.17	1.6354	0.1661	1.599
2-DLug1a2	0.01	0.5	0.006875	0.6875	3.75	0.2313	1.5739	0.2212	1.505
2-DLug2a	0.025	0.5	0.017188	0.6875	3.75	0.3291	1.4164	0.3047	1.311
2-DLug2a	0.05	0.5	0.034375	0.6875	3.75	0.4049	1.2322	0.3676	1.119

2-DLug2a	0.1	0.5	0.06875	0.6875	3.75	0.4592	0.9881	0.414	0.891
2-DLug3	0.15	0.5	0.103125	0.6875	3.75	0.473	0.831	0.4267	0.75
2-DLug3	0.2	0.5	0.1375	0.6875	3.75	0.4804	0.731	0.437	0.665
2-DLug3	0.25	0.5	0.171875	0.6875	3.75	0.4839	0.6585	0.4421	0.602
2-DLug3	0.3	0.5	0.20625	0.6875	3.75	0.4868	0.6047	0.4462	0.554
2-DLug4	0.35	0.5	0.240625	0.6875	3.75	0.4902	0.5638	0.4518	0.52
2-DLug4	0.4	0.5	0.275	0.6875	3.75	0.4957	0.5333	0.4589	0.494
2-DLug4	0.45	0.5	0.309375	0.6875	3.75	0.5029	0.5101	0.4679	0.475
2-DLug4	0.5	0.5	0.34375	0.6875	3.75	0.5124	0.493	0.4791	0.461
2-DLug4	0.55	0.5	0.378125	0.6875	3.75	0.5244	0.4811	0.4931	0.452
2-DLug4	0.6	0.5	0.4125	0.6875	3.75	0.5397	0.4741	0.5107	0.449
2-DLug4	0.65	0.5	0.446875	0.6875	3.75	0.5592	0.472	0.533	0.45
2-DLug4	0.7	0.5	0.48125	0.6875	3.75	0.5846	0.4754	0.5618	0.457
2-DLug4	0.75	0.5	0.515625	0.6875	3.75	0.6185	0.486	0.5999	0.471
2-DLug4	0.8	0.5	0.55	0.6875	3.75	0.6675	0.5078	0.654	0.498
2-DLug4	0.85	0.5	0.584375	0.6875	3.75	0.7404	0.5464	0.7336	0.541
2-DLug4	0.9	0.5	0.61875	0.6875	3.75	0.8654	0.6207	0.8677	0.622
2-DLug4	0.95	0.5	0.653125	0.6875	3.75	1.153	0.8049	1.1695	0.816
2-DLug1a2	0.005	0.5	0.005	1	5	0.1691	1.349	0.1698	1.354
2-DLug1a2	0.01	0.5	0.01	1	5	0.2262	1.276	0.221	1.247
2-DLug2a	0.025	0.5	0.025	1	5	0.3092	1.1031	0.2917	1.041
2-DLug2a	0.05	0.5	0.05	1	5	0.3611	0.9111	0.3354	0.846
2-DLug2a	0.1	0.5	0.1	1	5	0.3834	0.6841	0.3563	0.636
2-DLug3	0.15	0.5	0.15	1	5	0.3797	0.5532	0.3547	0.517
2-DLug3	0.2	0.5	0.2	1	5	0.3758	0.4741	0.3536	0.446
2-DLug3	0.25	0.5	0.25	1	5	0.372	0.4198	0.3517	0.397
2-DLug3	0.3	0.5	0.3	1	5	0.3698	0.3809	0.3511	0.362
2-DLug4	0.35	0.5	0.35	1	5	0.3693	0.3522	0.3523	0.336
2-DLug4	0.4	0.5	0.4	1	5	0.3711	0.331	0.3552	0.317
2-DLug4	0.45	0.5	0.45	1	5	0.3748	0.3152	0.3599	0.303
2-DLug4	0.5	0.5	0.5	1	5	0.3806	0.3037	0.3667	0.293
2-DLug4	0.55	0.5	0.55	1	5	0.3886	0.2957	0.3758	0.286
2-DLug4	0.6	0.5	0.6	1	5	0.3994	0.2909	0.3877	0.282
2-DLug4	0.65	0.5	0.65	1	5	0.4135	0.2893	0.4032	0.282
2-DLug4	0.7	0.5	0.7	1	5	0.4321	0.2914	0.4236	0.286
2-DLug4	0.75	0.5	0.75	1	5	0.4574	0.298	0.451	0.294
2-DLug4	0.8	0.5	0.8	1	5	0.4941	0.3117	0.4902	0.309
2-DLug4	0.85	0.5	0.85	1	5	0.5486	0.3357	0.548	0.335
2-DLug4	0.9	0.5	0.9	1	5	0.6421	0.3819	0.646	0.384
2-DLug4	0.95	0.5	0.95	1	5	0.8554	0.4952	0.8662	0.501

4.5 Challenges

This chapter documents results from the finite element simulations that use cosine bearing stress to model the load transfer between a pin and a lug. This is merely one method of five available in StressCheck[®] (the other four being linear springs, nonlinear springs, fastener models, and contact mechanics); however, it is very difficult to determine which is the most ‘correct’ model (if such a modeling approach even exists). Measuring stresses around a loaded lug hole is very difficult even in a laboratory with carefully controlled conditions, much less on an actual structure in service. There are methods such as photoelasticity that could be used to measure strains at the surface, should resources be available to conduct an experimental program. Validation of whatever model one chooses to model pin-lug load transfer is a resource-intensive process, and the wide variety of lug-pin mechanical interactions (neat-fit, bushed, cold-worked, etc.) in practice make model validation a difficult procedure.

4.6 Limitations

Only two-dimensional finite element results are presented; 3-D pin-lug load transfer is much more difficult to simulate and even less is known about the 3-D stress field on a loaded hole.

4.7 Recommendations

The library of Stress Intensity Factors for single Through Cracks in Lugs has been expanded to include bearing stress models of pin-lug load transfer. The question that remains is what method of modeling the pin-lug load transfer is closer to typical aerospace lugs: bearing stress, linear springs, nonlinear springs, fastener models, or contact models? This question likely could be answered by a substantial experimental program that uses photoelasticity and other methods to visualize stress or strain distributions in situ.

The Appendix contains further information on the applicability of these modeling techniques to experiments.

5. 3-D Lug Finite Element Solutions: Distributed Springs

5.1 Objective

The objective of this study was to compute a matrix of accurate and reliable Mode I SIFs for three-dimensional lugs, each with a single part-through crack at the hole, in the case of the pin load transfer being modeled as normal springs distributed around half of the lug hole. These solutions supplement a 3-D lug solution database that was produced in 2004, in which the pin load transfer was modeled with a cosine bearing traction on the hole bore.

5.2 Approach

Lugs can be found in many different substructures in an aircraft: wing attach fittings and control linkages among others. AFGROW currently contains a model for a single Part-through Crack in a 3-D Lug. However, users of this AFGROW crack growth model in the past have indicated that the results from the AFGROW analyses can be suspect; therefore, adding to the expanded lug solutions was a major goal of this project.

The load transfer between a pin (neat fit) and a stout lug was modeled with the Figure 8. The *p*-version finite element method software StressCheck[®] (ESRD, St. Louis, MO) was used to simulate the interaction of a lug with a load transfer pin; the goal of the analyses was to provide tabulated tables of accurate and reliable Mode I (SIFs) for a Part-through Corner Crack in a 3-D Lug for eventual incorporation into existing AFGROW databases. All 3-D FEMs are subjected to a constant normal traction at the attachment boundary (left side in Figure 8); displacement of the hole is constrained by normal springs distributed 180 degrees around the hole, Figure 9. The normal spring constant K_n is estimated from the hole diameter and the pin material parameters, Equation (3). The results from these models are designed to round out the existing AFGROW database of 3-D lug solutions that used the spring constraint to model the pin-lug load transfer.

$$K_n = \frac{2E_{pin}}{D(1+\nu)(1-2\nu)} \quad (3)$$

where: E_{pin} is the Young's modulus of the pin, $E_{pin} = 3E_{lug}$,

D is the hole diameter, and

ν is the Poisson ratio of the pin (taken to be the same as that of the lug).

5.3 Schematic

Three dimensional finite element models of single part-through cracks at a loaded hole in a lug were modeled with StressCheck[®]. The pin-lug load transfer was modeled with normal springs with spring constant defined by Equation (3) and distributed over 180 degrees of the hole; Figures 8 and 9 are schematics of the model, load and constraints of the lug. A typical StressCheck FEMs is shown in Figure 10.

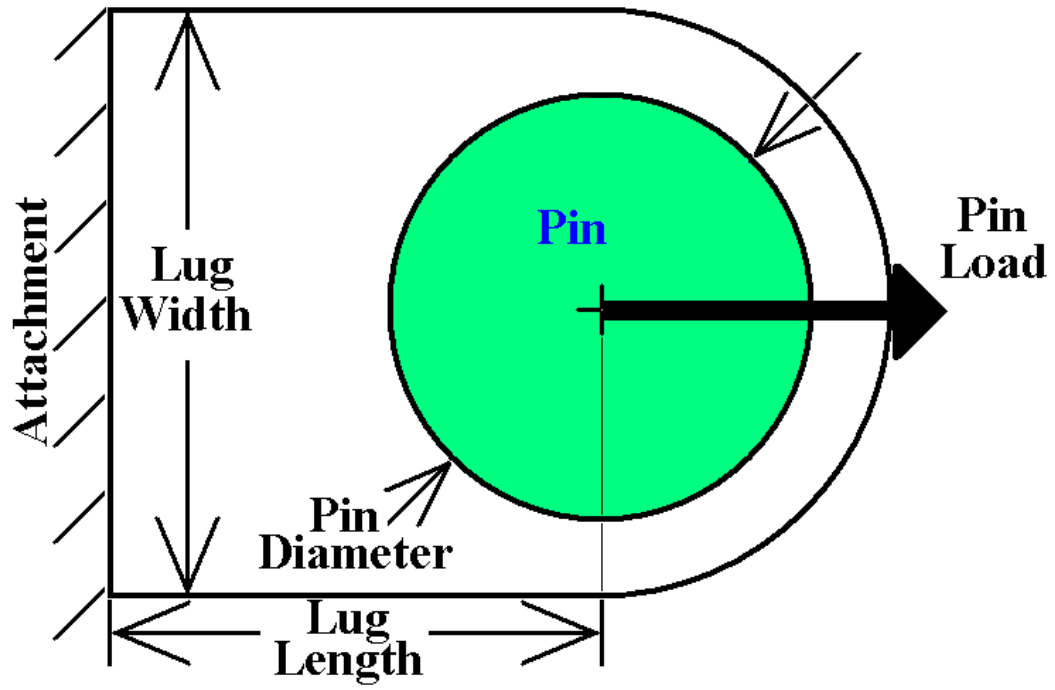


Figure 8. Pin-Lug Load Transfer Idealization.

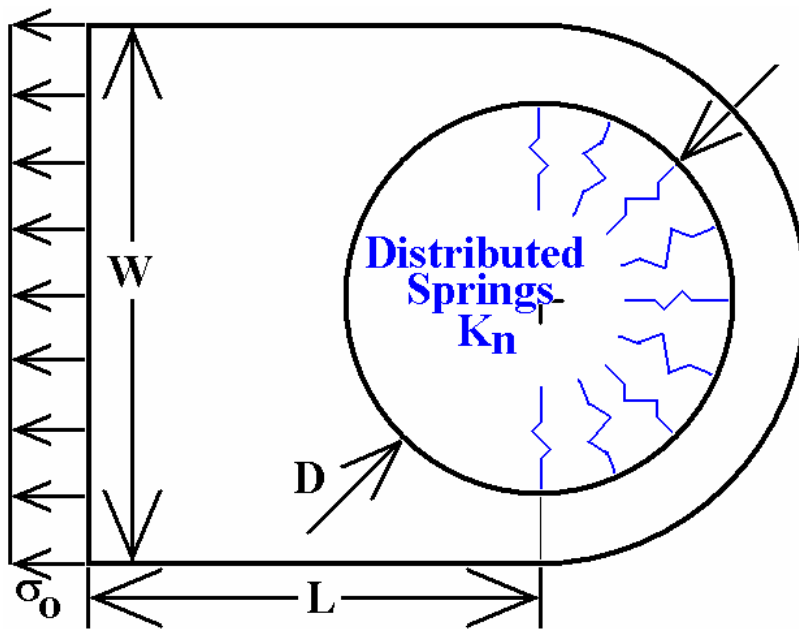


Figure 9. Lug Geometry, Loads, and Spring Constraints

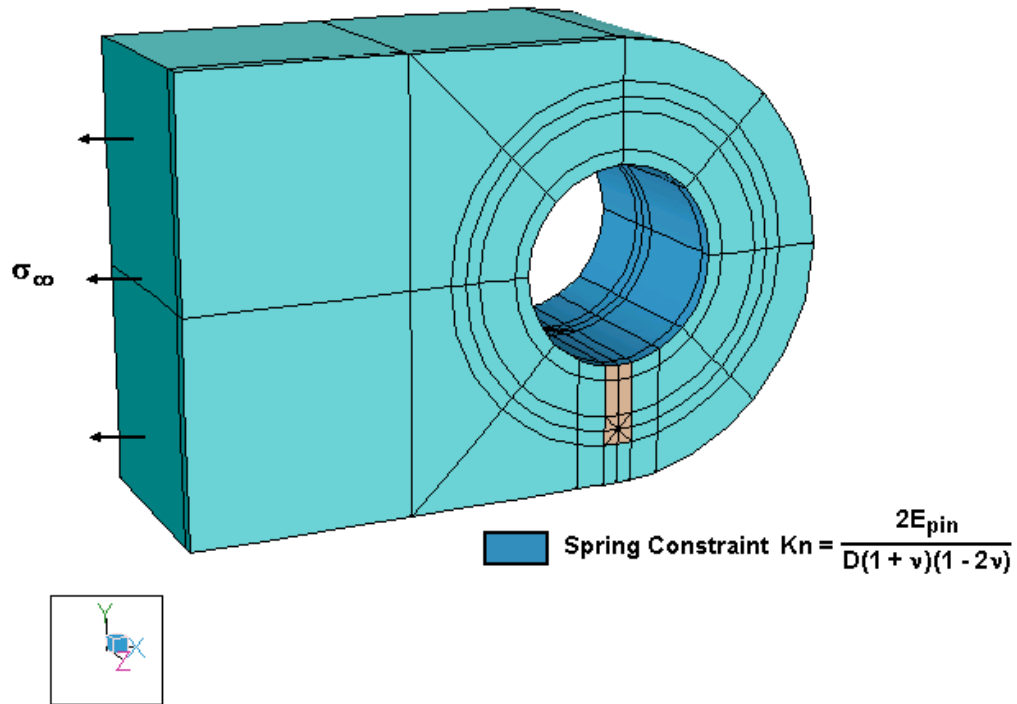


Figure 10. Representative StressCheck Model of Part-through Crack at Loaded Hole in a Lug

5.4 Results

The range of parameters in the finite element simulations is outlined in Table 5. Over 600 three-dimensional finite element solutions were required to obtain adequate Stress Intensity Factors for this range of parameters. Fortunately, the same parameter variations were explored for 3-D lugs in 2004, except the pin-lug load transfer was modeled with cosine bearing stress. The analyst typically only had to change the load and boundary constraints on each finite element model constructed in 2004 to get the new solutions for normal spring constraints. There were some new models constructed, partially in response to customer request to add another W/D . Since over 600 solutions were computed, data will not be presented in this report but has appeared in spreadsheets forwarded to the U.S. Air Force customers.

Table 5. Range of Parameters for a Lug Part-Through Crack

Parameter	Description	Range
<i>a</i>	Bore Crack Length, in.	$0.005T \leq a \leq 0.9T$
<i>c</i>	Surface Crack Length, in.	$0.005 \leq c \leq 1.8$
<i>D</i>	Hole Diameter, in.	$0.25T \leq D \leq 4T$
<i>T</i>	Thickness, in.	No limit
<i>W</i>	Lug Outer Diameter	$1.3D \leq W \leq 5D$

5.5 Challenges

This chapter documents results from the finite element simulations that use distributed normal springs to model the load transfer between a pin and a lug in three dimensions. This is merely one method of four 3-D methods available in StressCheck[®] (the other three being linear springs, nonlinear springs, and contact mechanics), however, it is very difficult to determine which is the most ‘correct’ model (if such a modeling approach even exists). Measuring stresses around a loaded lug hole is very difficult even in a laboratory with carefully controlled conditions, much less on an actual structure in service. There are methods such as photoelasticity that could be used to measure strains at the surface, should resources be available to conduct an experimental program. Validation of whatever model one chooses to model pin-lug load transfer is a resource-intensive process, and the wide variety of lug-pin mechanical interactions (neat-fit, bushed, cold-worked, etc.) in practice make model validation a difficult procedure.

Over 600 (3-D) finite element analyses (FEAs) were needed to construct part-through cracks in lugs for a wide range of parameter variations—most of the required models were created during 2004 funding for this project (a few new ones were required in 2005), and therefore these models already met stringent accuracy goals; in the final tally of all models needed to span the entire range, only 8 models were needed. Nevertheless, these models represent several months of development by an experienced finite element analyst. The solution quality estimate (the percentage difference between the best external-K solver solution and a solution extrapolated to an infinite number of degrees of freedom using a Richardson extrapolation of the three best p-level solutions) in general, was excellent. Of the 681 total solutions, 635 (93.2 percent) had a solution quality estimate less than 1 percent, 43 (6.3 percent) had a solution quality estimate between 1 percent and 2 percent, and only 3 (0.4 percent) had a solution quality estimate over 2 percent. The 46 solutions above 1 percent are generally at geometric parameter combinations that would be considered extreme, or atypical of standard industry design practice.

Since fracture mechanics parameters are calculated from a finite number of tables, interpolation and extrapolation are very important considerations—clearly one wants the interpolation and extrapolation error to be ‘small’, however large one defines ‘small’ error to be. There are actually two notions to consider when choosing the interpolation scheme: does one choose linear or higher order interpolation; and which ‘hard points’ will be used to define the curves which are used in the interpolation. ‘Hard points’ are the specific parameter combinations where finite

element solutions were run and whose results were collected in the tables that are to be used in the interpolations. For instance, the ‘hard points’ in the tables from 2004 consisted of several points ranging from ratios of lug width to hole diameter of $W/D = 1.3$ to $W/D = 5.0$. Testing in 2005 resulted in a call for an additional hard point of $W/D = 1.4$ to decrease the interpolation error. In response to that call, additional cases were run at $W/D = 1.4$ for both the cosine bearing loads (all other variations on W/D were completed in 2004) and the distributed spring constraints.

5.6 Limitations

The user can vary the parameters in the part-through crack in lug models over a theoretically infinite range—if fracture mechanics data is needed for geometries outside the range of the geometry combinations that were used to define the tables in the table look up, AFGROW merely extrapolates using the defined tables. However, if the analyst chooses to use parameter values outside the ranges indicated in the table, numerical accuracy in the FEMs might suffer unacceptably.

Very little is known about the 3-D stress field around a loaded hole; 3-D pin-lug load transfer is very difficult to simulate and even less is known about the 3-D stress field on a loaded hole than about the 2-D stress field on a loaded hole.

5.7 Recommendations

The library of Stress Intensity Factors for single Part-through Cracks in 3-D Lugs has been expanded to include distributed spring models of pin-lug load transfer. The question that remains is what method of modeling the pin-lug load transfer is closer to typical aerostructure lugs: bearing stress, linear springs, nonlinear springs, or contact models? This question probably could be answered by a substantial experimental program that uses photoelasticity and other methods of visualize stress or strain distributions in situ.

The Appendix contains further information on the applicability of these modeling techniques to experiments.

6. Lug Boundary Condition Effects: Bearing Reactions and Interference Fits

6.1 Objective

Lugs are very important substructures in aircraft, being used to attach critical structures such as wings and landing gear. Determination of the damage tolerance of lugs depends on reliable estimates of the stresses near the lug hole. Typically these estimates are taken from finite element solutions or from curve fits of finite element solutions. A critical part of the lug model is a physically realistic model for the interaction of the pin with the lug. The goal of this study was to obtain accurate and reliable computed stresses from finite element models that use various boundary conditions for simulating the pin-lug interaction and to document the differences in the computed stresses due to these methods. These boundary conditions included fasteners, linear and nonlinear spring constraints, and bearing stress loads. Additionally, fasteners were simulated with and without interference fits.

6.2 Approach

The load transfer between a pin (neat or interference fit) and a stout lug was modeled with the finite element method, Figure 11. The *p*-version finite element method software used for this study, StressCheck[®] (ESRD, St. Louis, MO), simulated the interaction of a lug with a load transfer pin (frictionless interaction modeled). The goal was to obtain accurate and reliable stresses on the plane where cracks typically form. StressCheck[®] has a number of boundary condition options (see Table 6) in two-dimensions (2-D) for modeling the interaction of a pin loaded lug. Also shown in Table 6 are the load and constraint pairs that are used in each Boundary Condition type, as well as the kinematics (linear or nonlinear) for that Boundary Condition.

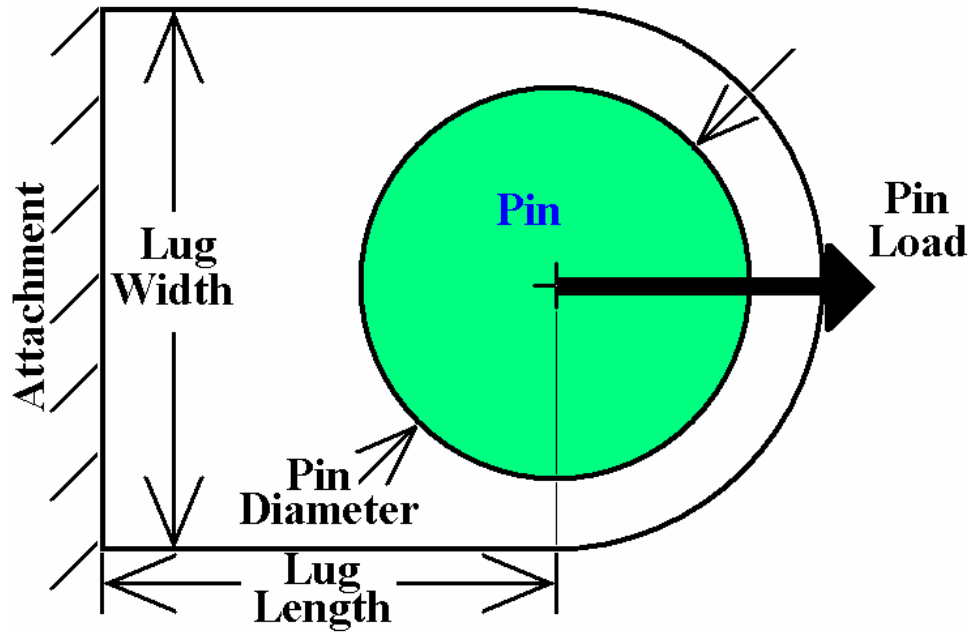


Figure 11. Load Transfer with a Pin in a Stout Lug

Table 6. Loads and Constraints for Various Lug/Pin Boundary Conditions

Boundary Condition	Load	Constraint	Kinematics
Fastener	Constant tension on far field boundary	Fastener	Nonlinear
Linear springs	Constant tension on far field boundary	Normal springs, 180 degrees around hole	Linear
Nonlinear springs	Constant tension on far field boundary	Normal springs, 360 degrees around hole	Nonlinear
Bearing stress load	Bearing stress on lug hole	Symmetry on far field boundary	Linear

The stresses from StressCheck[®] finite element models with the four Boundary Conditions (bearing stress load, linear springs, fastener, and nonlinear springs) were computed and used to compare the four models. In addition, pins or fasteners that are larger than the lug hole will be modeled with interference fit boundary constraints in the fastener models. The question of what the ‘correct’ answer is left open, and depends on experimental results. In general, the linear springs, nonlinear springs, and fastener boundary condition models are relatively similar in their idealization of reality, the bearing stress load condition is the odd method out. This difference is typically reflected in the results: the first three modeling approaches produce similar results, where as the bearing stress modeling approach often produces results that significantly differ from the other three approaches.

6.3 Lug-Pin Model Schematics

Figures 12-14 show schematically the lug models that were analyzed; each model differs from the others by the method used to model the load transfer between the pin and the lug. Figure 12 shows the model of the pin as a fastener, which can resist normal traction on the boundary of the fastener and the hole, but cannot resist shear traction on the hole. The pin load is modeled as the reaction of the fastener to the application of a constant normal traction at the left boundary of the model of Figure 12. Figure 13 shows the model of the pin as normal springs distributed around half the hole. Again, the pin load is modeled as the reaction of (this time) the normal springs to a constant normal traction at the left boundary of Figure 13. While Figure 13 shows the springs distributed around only half the hole, spring models that distributed around the entire hole were also computed (note that a nonlinear iteration of the finite element solution is needed to model the pin as springs around the entire hole; this is so that the normal springs ‘break free’ of the hole surface when the normal traction is greater than or equal to 0.0, that is, in tension); these results in all cases were equivalent to the fastener model results, Figure 12. Figure 14 shows the Bearing Load with symmetry at the far field boundary. The Bearing Load models the pin-lug interaction as a cosine distributed normal traction $A\cos(\theta)$ on the interior of the hole; the magnitude and direction of the pin load is specified *a priori*. The Fastener and Springs idealizations model the pin-lug interaction as the reaction of the fastener or springs to the application of a load at far field; the magnitude and direction of the pin load are not known *a priori*, but must be computed after the finite element solution is completed. Whenever possible, all cases used far field normal traction σ_0 of 1 ksi, so that the bearing stress can be computed:

$$\sigma_{bear} = \frac{\sigma_0 W}{D} = \frac{W}{D} \quad (4)$$

where: W is the width of the lug and

D is the diameter of the hole.

The normal spring coefficient K_n for all spring models is estimated with the following formula:

$$K_n = \frac{2E_{pin}}{D_{pin} [1 + \nu_{pin}] [1 - 2\nu_{pin}]} \quad (5)$$

where: E_{pin} is the Young's modulus of the pin or fastener,

ν_{pin} is the Poisson ratio of the pin or fastener, and

D_{pin} is the diameter of the hole, equal to the diameter of the pin or fastener if the interference level is zero (0.0).

The function used to define the bearing stress traction σ_n shown in Figure 14 is following:

$$\sigma_n = A \cos(\theta) = \frac{4P}{\pi D t} \cos(\theta) \quad (6)$$

where: P is the pin or fastener load,

t is the thickness of the lug, and

θ is the angle around the hole, with $\theta = 0$ deg. is the horizontal (Figures 12-14), and the bearing stress is defined nonzero in the interval $-90 \text{ deg.} \leq \theta \leq 90 \text{ deg.}$

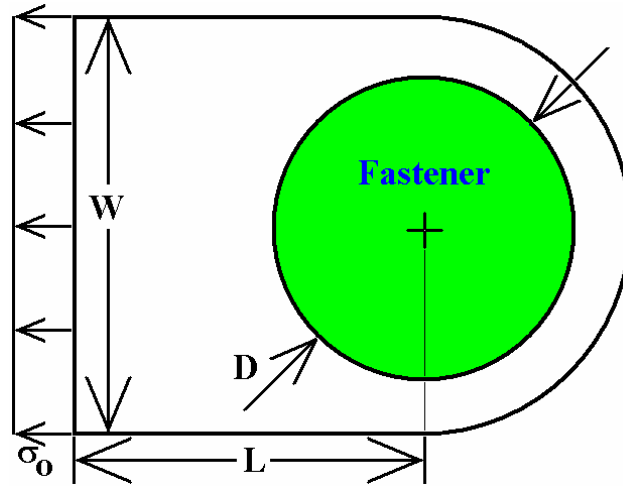


Figure 12. Lug Model for Fastener

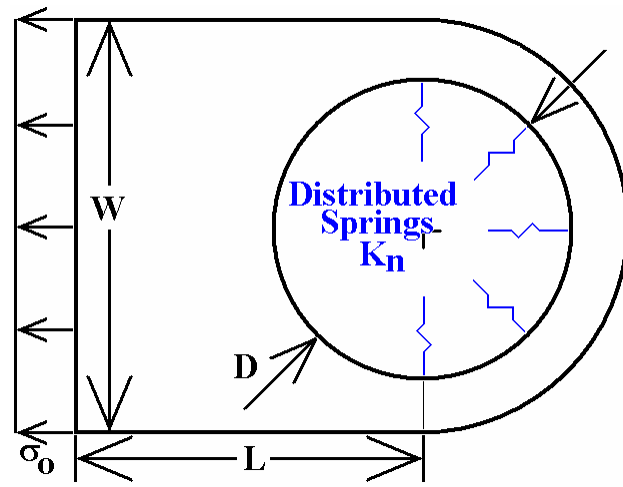


Figure 13. Lug Model for Linear Springs Boundary Condition

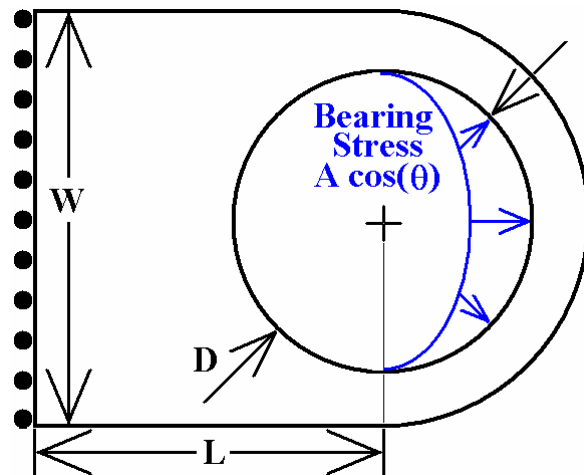


Figure 14. Lug Model for Bearing Stress Load

The dimensions of the various parameters are shown in Table 7 below. All lugs were modeled as aluminum, while all fasteners and springs were modeled as steel, which has a Young's modulus approximately 3 times the aluminum Young's modulus. The Poisson ratio of both aluminum and steel are close to 0.3, so this value was used for all simulations.

Table 7. Model Parameter Dimensions

Parameter	Definition	Value	Variable?
σ_0	far field stress, ksi	1.0	No
W	lug width, in.	1.3, 1.5, 2.0, 5.0	Yes
D	hole diameter, in.	0.5	No
L	lug length, in.	W	Yes
δ/D	diametrical interference level	0.0, 0.0001, 0.0005, 0.001, 0.005, 0.01	Yes
E_{plate}	Young's modulus of plate (lug), ksi	10000	No
ν_{pin}	Poisson ratio of plate (lug)	0.3	No
E_{pin}	Young's modulus of pin (fastener), ksi	30000	No
ν_{pin}	Poisson ratio of pin (fastener)	0.3	No

The diametrical interference levels δ/D indicated in Table 7 model fasteners or pins that have diameters that are larger than the diameters of the hole, and are designed to cover a wide range of

anticipated interference levels that might be seen in manufacturing of these lugs and pins. The results using the interference levels are difficult to interpret; the simulation requires nonlinear iterations, as the finite element software tries to find the regions of contact between the pin/fastener and the lug hole (a region of contact is any place the radial stress between the pin and the hole is compressive, that is, negative) and this region of contact is highly dependent on the magnitude of the pin load (equivalently, the magnitude of the applied far field stress). For this study, all far field stresses are fixed to 1 ksi; for the high interference levels, $\delta/D > 0.0005$, the pin never completely breaks away from the hole, that is, there is compressive radial stress everywhere on the hole surface.

6.4 Results

The primary engineering data used to compare competing models for pin-lug load transfer are the normal stresses S_{xx} from the edge of the hole to the edge of the lug, Figure 15, along the ray y' . The stresses S_{xx} are in the same direction as the pin load, which is the same direction as the far field stress. The ray y' is on the plane where cracks are anticipated.

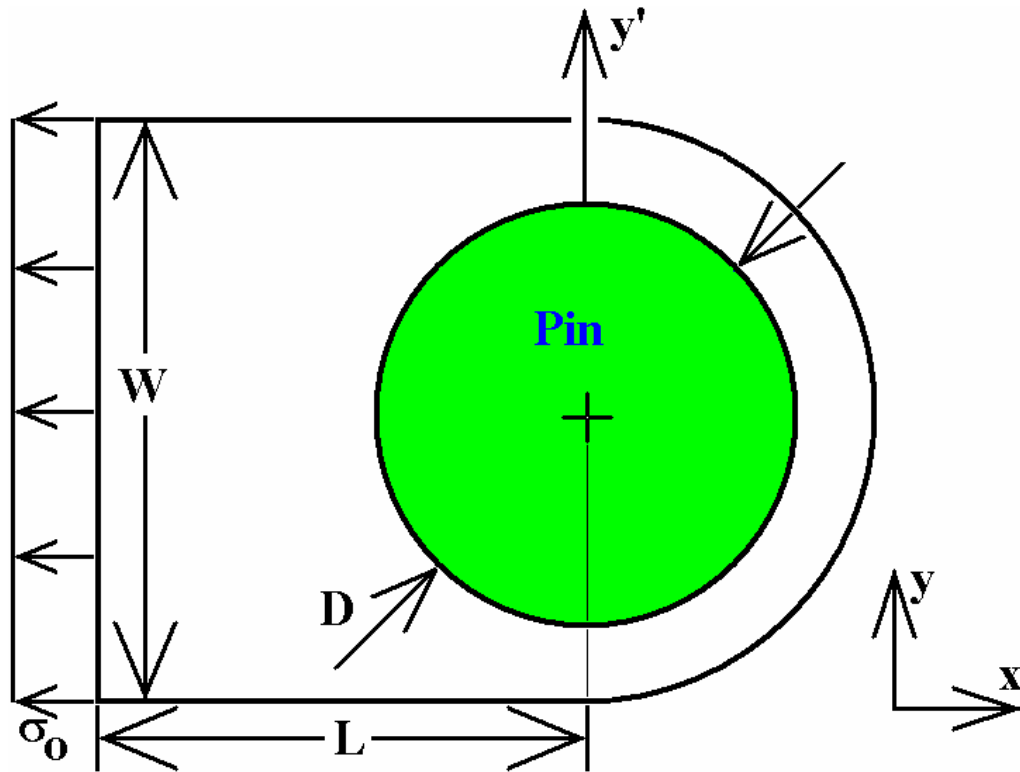


Figure 15. Lug Model Showing Location of Stresses Used for Comparisons

6.4.1 Radial Stress Distributions

Each of the methods for modeling the pin load transfer to the lug generally as a rule results in a different radial stress on the hole surface, Figure 16, which shows the radial stresses for the smallest lug, $W/D = 1.3$. The only exception to this rule are the nonlinear springs and fastener models; both give you almost exactly the same radial stress distribution on the hole surface. The bearing stress model gives you the cleanest radial stresses, because the bearing stress model specified the radial stresses on the hole surface as a load. Each of the other models yield radial stresses that drop to and hover around zero for some part of the hole; the oscillations that are apparent in Figure 16 are numerical artifacts which can be reduced by significantly increasing the number of elements near the hole.

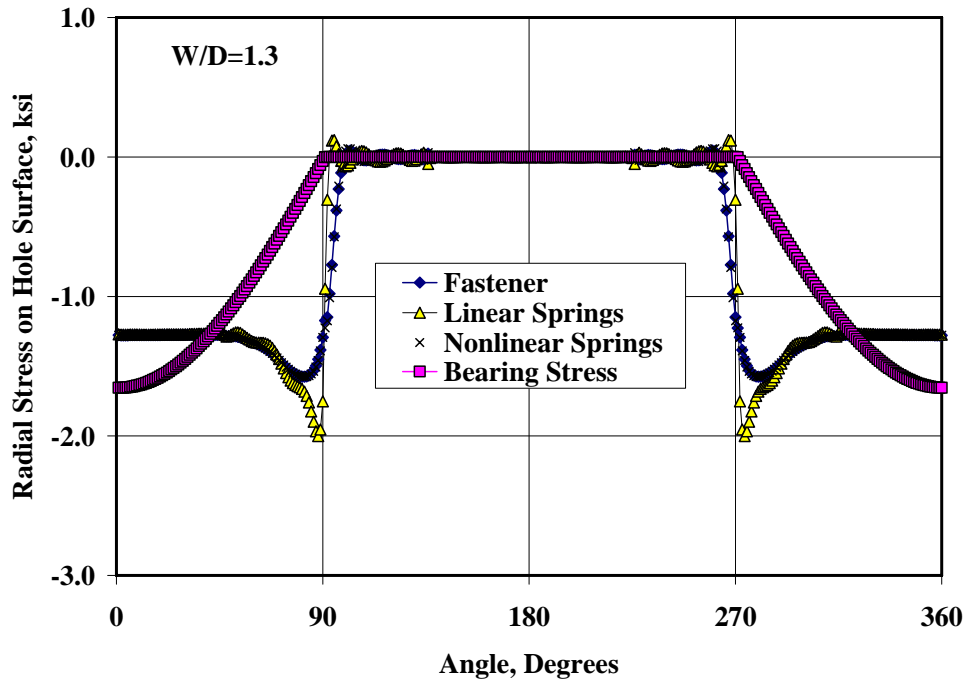


Figure 16. Radial Stresses on Lug Hole, $W/D = 1.3$ Fastener is ‘neat fit’, $\delta/D = 0$

In all cases, the pin or fastener is modeled as one that is 3 times stiffer than the lug or plate, that is $E_{pin}/E_{plate} = 3$. Not shown are results from simulations in which the pin Young’s modulus E_{pin} is progressively decreased until the ratio of the pin to the plate Young’s modulus is $E_{pin}/E_{plate} = 1/1000$; as this ratio decreases from 3 to 0.001, the radial stress distributions of the fastener models gradually become aligned with the radial stress from the Bearing Stress model at this $W/D = 1.3$. The same effect can be demonstrated by gradually increasing W/D to 5 or greater. This could lead one to the conclusion that as either the pin modulus or the effective pin modulus (as the fit of the pin to the lug becomes loose, the effective pin modulus goes down) decreases, the bearing stress modeling approach produces better results.

6.4.2 Normal Stress From Hole Edge

6.4.2.1 Comparison of Four Models for Neat Fit Fasteners

The normal stress from the edge of the hole to the edge of the lug (‘vertical’ in Figure 15) is compared for the four (4) methods for modeling the pin-lug interaction. The Fastener Model features a ‘neat fit,’ that is, the diametrical interference is $\delta/D = 0$.

The normal stresses from the hole edge are compared for each model at four W/D , $W/D = 1.3, W/D = 1.5, W/D = 2.0$ and $W/D = 5.0$ in Figure 17 below. There are large differences in the normal stresses at $W/D = 1.3$; these differences gradually decrease until they are negligible by $W/D = 5.0$. What is clear from these figures is that the results from the

Bearing Stress model are very different from the results of the other three; in fact, the results from the Fastener, Linear and Nonlinear Spring models appear to be very close (the Fastener model is mechanically similar to the Nonlinear Spring model, so one would expect the stresses computed using these two models would be very close).

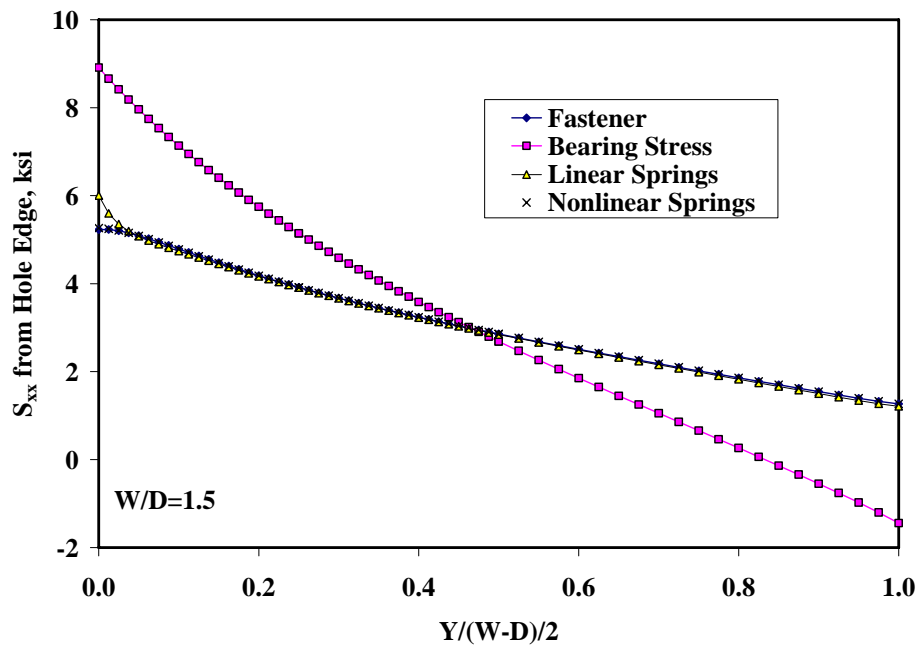
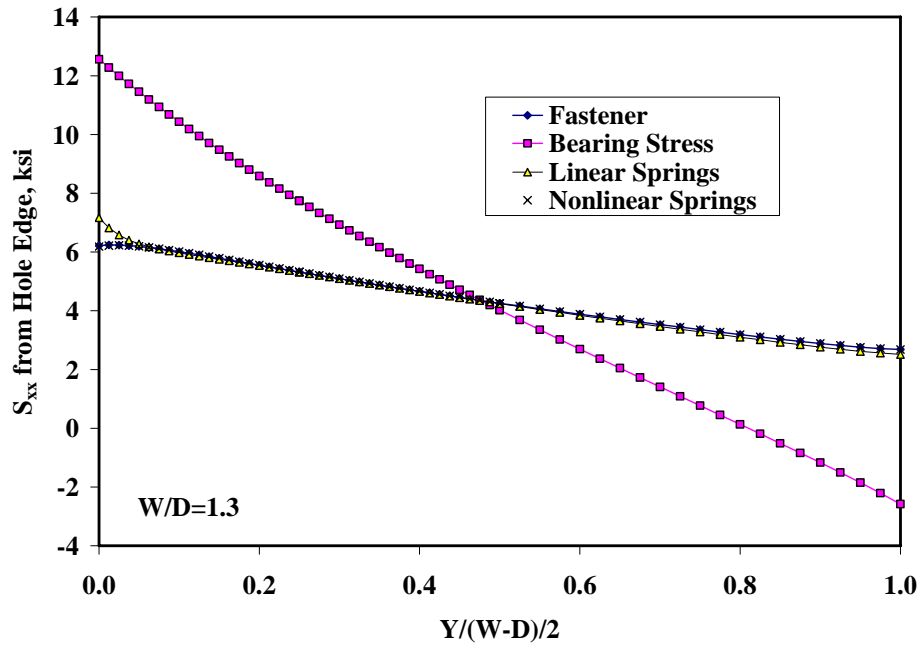


Figure 17. (a/b) Normal Stresses from Hole Edge to Lug Edge

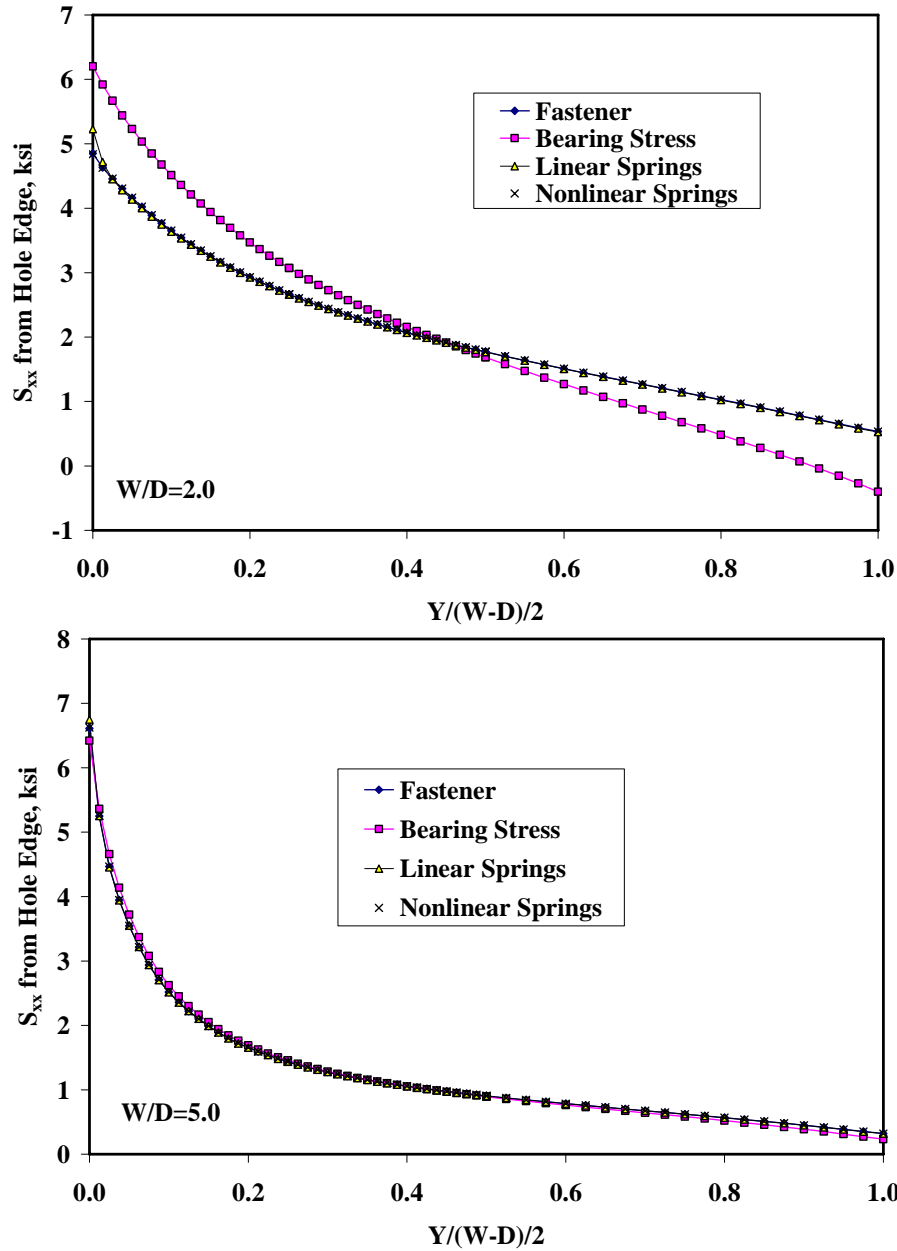


Figure 17 (c/d). Normal Stresses from Hole Edge to Lug Edge

6.4.2.2 Comparison of Interference Fit Levels

The Fastener Model (Figure 12) was used to simulate interference fit fasteners, in which the fasteners are incrementally larger than the lug hole prior to installation (the fastener might be forced into the hole, or chilled to decrease its diameter and then slid into the hole). The interference level is determined by the ratio of the difference between the diameters of the pin

and the lug hole and the diameter of the lug hole, δ/D . For this study, the diametrical interference was varied from 0 ('neat fit') to 0.01, $\delta/D = 0, 0.0001, 0.0005, 0.001, 0.005, 0.01$. The diameter of the hole D was again fixed at 0.5 in. and the far field stress σ_0 was 1 ksi for all simulations; this far field stress was arbitrarily chosen, and had a significant effect on the results—because the problem is nonlinear, requiring nonlinear iterations to define the regions of contact between the fastener and the lug hole, the stresses are nonlinearly dependent on the applied far field stress, and therefore cannot be linearly scaled for larger far field stresses. All simulations used the smallest lug width, $W/D = 1.3$.

The radial stresses on the hole are plotted as a function of the interference levels in Figure 18. The radial stress drops to zero over some portion of the hole for 'low' levels of interference, that is, for $\delta/D \leq 0.0005$. For all greater interference levels, the pin never breaks away from the hole over any portion of the hole, apparent from the compressive radial stresses over the entire hole surface.

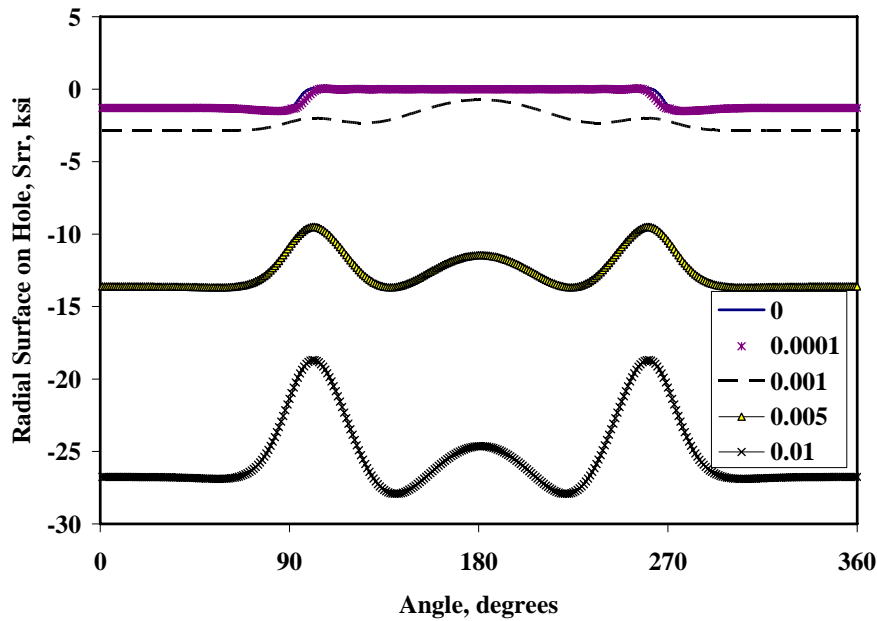


Figure 18. Radial Stresses on Hole Surface, $\delta/D = 0, 0.0001, 0.001, 0.005, 0.01$

To show the transition from the very low levels of interference to higher levels of interference, the radial stress for $\delta/D \leq 0.001$ are shown in Figure 19 below. Because the far field stress is so small, 1 ksi, even for a 'small' interference level $\delta/D = 0.001$ (that's 1/1000th of the diameter), the pin and the hole do not separate over any portion of the hole. However, someplace between $\delta/D = 0.0005$ and $\delta/D = 0.001$, some portions of the pin do separate from the hole. For a much bigger far field stress, the pin will again separate from the hole over a portion of the hole at $\delta/D = 0.001$, Figure 20. The Radial stresses are normalized by the applied far field stress S_0 .

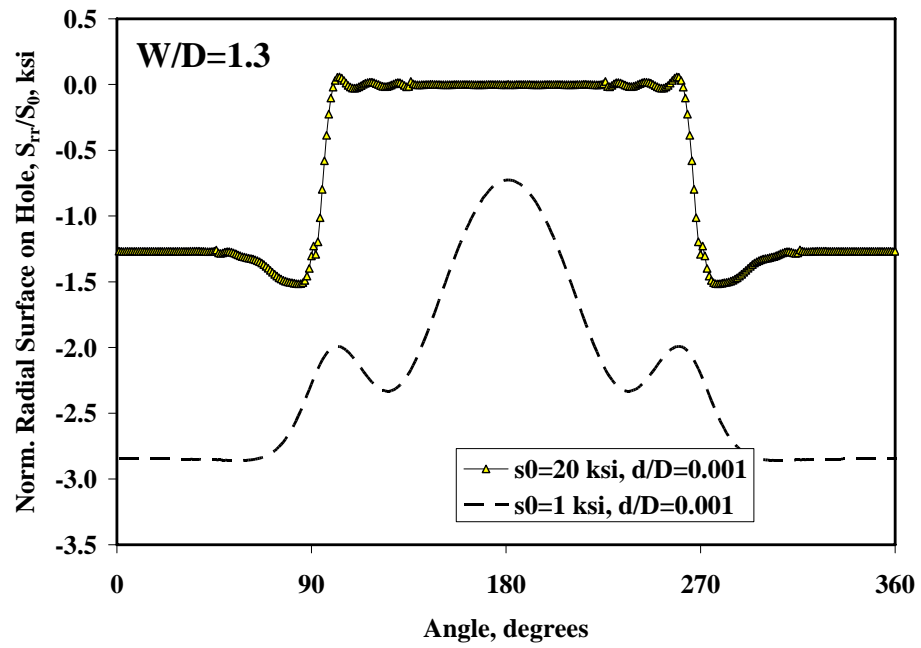


Figure 19. Radial Stresses on Hole Surface, $W/D=3$

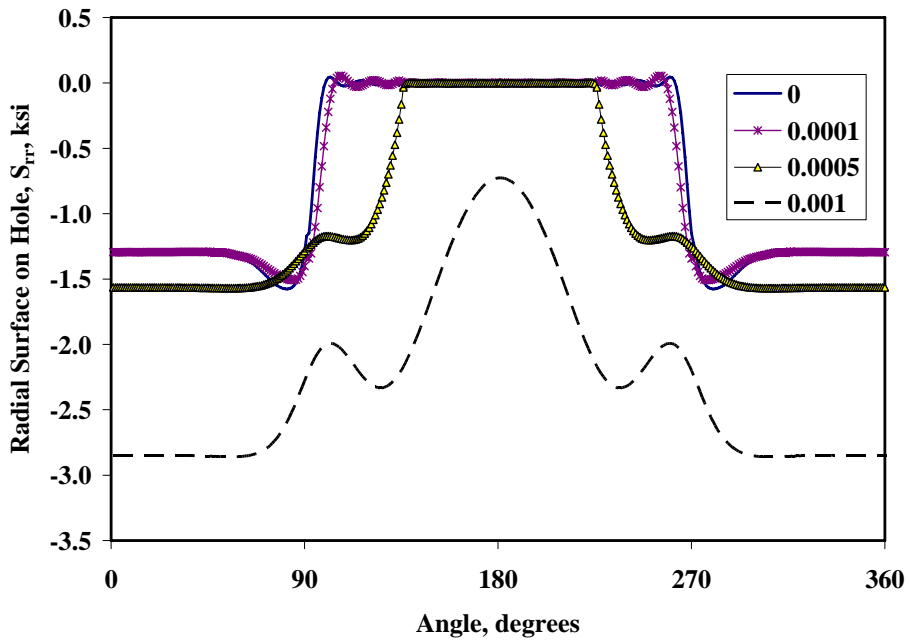


Figure 20. Radial Stresses on Hole Surface, $\delta/D = 0, 0.0001, 0.0005, 0.001$.

The normal stresses from the hole edge are shown in Figure 21 for a range of interference levels. The stresses are still fairly small for small interference levels, $\delta/D = 0.0005$, and start to increase substantially as the interference levels are increased from there. Note that the plate/lug material is linear elastic, so that no attempt was made to account for plasticity—the stress levels for the largest interference level $\delta/D = 0.01$, are obviously too large to be realistic.

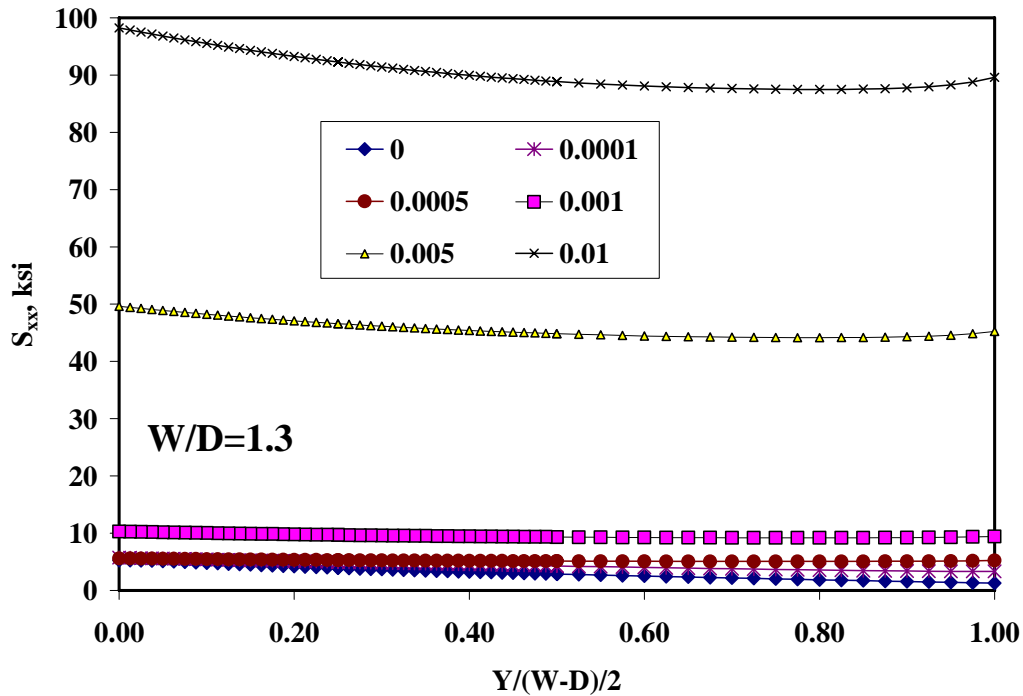


Figure 21. Normal Stresses from Hole Edge to Lug Edge

Figure 22 shows the same normal stresses, but focuses only the smallest interference levels, $\delta/D \leq 0.001$.

6.5 Challenges

This chapter documents results from the finite element simulation of four different methods for modeling the load transfer between a pin and a lug. Each method yields different results; however there appears to be no way of determining which is the correct model (if such a modeling approach exists) or even which model is better. Measuring stresses around the hole is very difficult even in a laboratory with carefully controlled conditions, much less on an actual structure in service. There are methods such as photoelasticity that could be used to measure strains at the surface, though we did not explore this experimental technique any further. Validation of whatever model you choose to model pin-lug load transfer is still problematic.

6.6 Limitations

Only two-dimensional finite element results are presented; three-dimensional pin-lug load transfer is much more difficult to simulate if there is an interference fit of the pin in the lug hole;

the method that the manufacturer uses to install the pin which is larger than the lug hole at room temperature entirely determines the highly three dimensional residual stresses that are caused in the lugs by the manufacturing procedure.

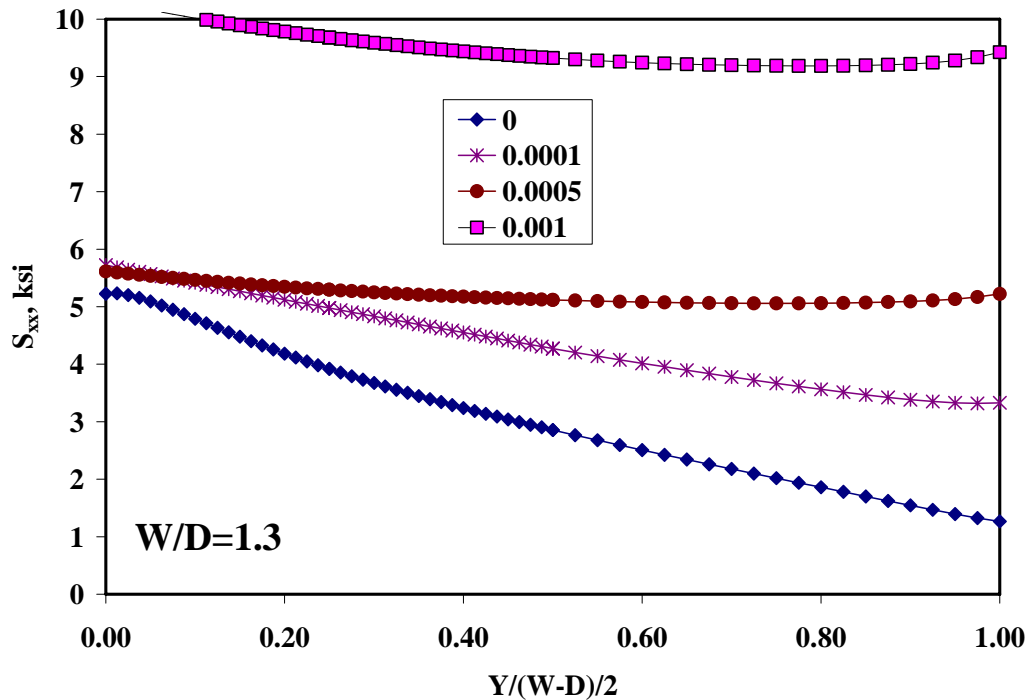


Figure 22. Normal Stresses from Hole Edge to Lug Edge for Small Interference

6.7 Conclusions and Recommendations

6.7.1 Conclusions

The effect of different methods for modeling pin-lug load transfer was determined by comparing radial stress on the hole surfaces and normal stresses from the edge of the hole to the edge of the lug. The following conclusions can be made:

- Nonlinear springs and fastener models are mechanically the same.
- There was little difference between the stresses from the linear spring, nonlinear spring and fastener models.
- There was a substantial difference between the stresses from the bearing load model and the other three models: fastener, linear spring and nonlinear spring.
- For small W/D geometries, the bearing stress model produces a more severe normal stress profile (the primary stresses that drive mode I cracks) than the other loading/boundary conditions in the initial stages of crack growth (smaller cracks) through the lug. This trend reverses as the crack lengths become longer.
- Results in which radial interference was modeled with the pin load transfer were very

difficult to interpret, perhaps precluding any meaningful conclusions; because radial interference modeling is a nonlinear kinematics problem. The extent of contact of the pin on the hole is not known *a priori*, and depends strongly on the applied pin load. Any engineering data extracted from the finite element solutions is nonlinearly dependent on the applied pin load.

6.7.2 Recommendations

The primary unknown during this modeling process is what the stresses around a loaded lug should look like. There appears to be substantial testing of lugs in the literature, however, very few researchers have attempted to measure the stresses or strains around a loaded hole.

Obviously due to the hidden location, the radial stress on the hole is next to impossible to determine. However, with techniques such as photoelasticity, it is possible that the strains and stresses could be measured on the lug surfaces.

The appendix contains further information on the applicability of these modeling techniques to experiments.

7. Support for Purdue Experimental Lug Tests

7.1 Objective

This chapter describes AP/ES' support of the experimental lug tests that were performed by Mr. Nic Moyle at Purdue University. This support was in the form of three-dimensional finite element solutions, each of whose goals was accurate Mode I Stress Intensity Factors for elliptical cracks located at straight holes that are in lugs. Both part-through and curved through (aka oblique) cracks with origins at the corner of the holes were modeled. In addition to the models presented here, 3-D finite element models were given to Purdue, and AP/ES provided support on proper use of these models, verification analyses to ensure that results from Purdue were sound and the models were being properly used, and guidance on correlation of analytical results to mechanical tests. Mr. Moyle will publish detailed documentation on this correlation for his M.S. thesis.

7.2 Approach

This supports the experimental test program carried out by Nic Moyle of Purdue University, who tested lugs of varying dimension with variable amplitude marker band spectra. Corner cracks were introduced at the hole-surface corner. Marker bands in the fatigue load spectra allowed the crack fronts to be tracked. A typical corner crack will get larger with each cycle until the bore crack front intersects the opposite surface (or back face) and transition to an 'oblique' crack, which is a curved through crack whose crack tips intersect the upper and lower surfaces of the lug with two different crack lengths. The finite element models of oblique cracks documented here were constructed so that what was observed in the marker bands could be modeled with more fidelity in the crack propagation than if the scenario that the corner crack immediately transitions to a straight through crack was hypothesized.

The loading of a three-dimensional lug with a constant far field normal traction was modeled with the finite element method. The *p*-version finite element method software that we used for this study, StressCheck[®] (ESRD, St. Louis, MO), was used to calculate Mode I SIFs for part-through and oblique cracks located at the corner of a hole which contains a pin to counteract the applied far field traction. A schematic of the lug model is depicted in Figure 23 below. Note that $a = 0.95T$ is a part-through crack, included to show the transition from part-through to through-crack behavior in this study.

A uniform tensile stress is applied 'far field' on one side of the lug (left side on Figure 23). A semi-elliptical through crack is located at the corner of the hole bore, in a plane perpendicular to the applied far field stress. To simulate the load transfer from a neat fit pin to the lug (equivalently, the response of a fixed pin to the applied load at the left of Figure 23), the lug is constrained by springs spanning a $-90.0 < \text{degrees} < 90.0$ angle. The lug geometry and parametric dimensions are also shown in Figure 23. A representative StressCheck[®] model is shown in Figure 24.

The parameters were varied as indicated in Table 8. The parameter variations were selected to demonstrate the effect the transition of a part-through crack (that is, the bore crack length is less than the lug thickness T) to an oblique crack (the bore crack length in Figure 23 is greater than

the lug thickness T) at the same surface crack length, $c = 0.1407$. The parameters in this table were chosen to model closely the lugs that were being tested at Purdue University, and to represent crack lengths near transition from a preliminary AFGROW analysis.

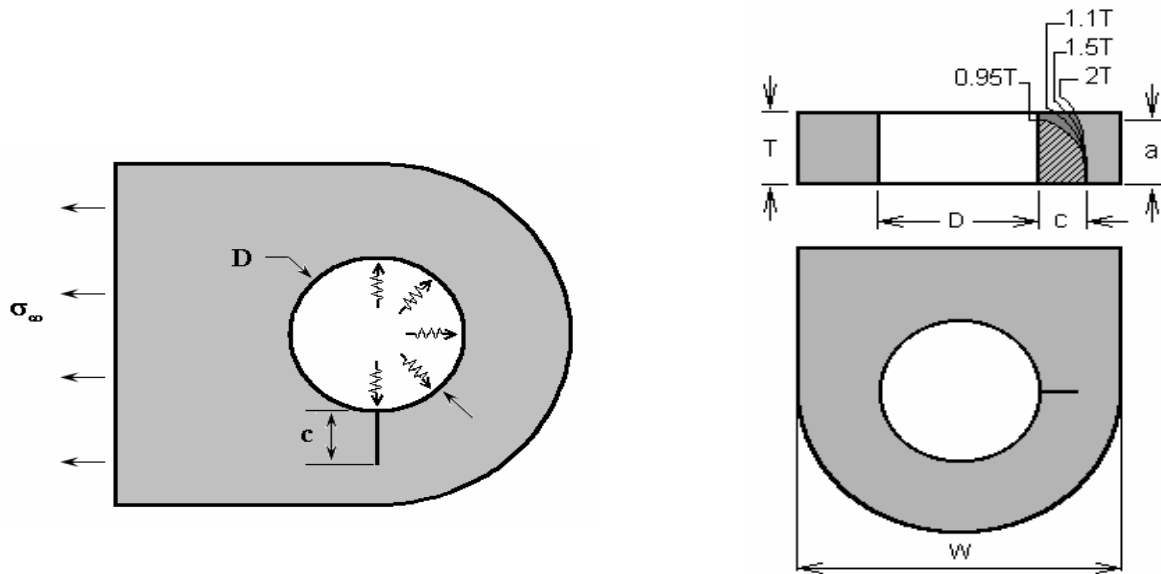


Figure 23. Lug Model Loading Configuration and Geometry

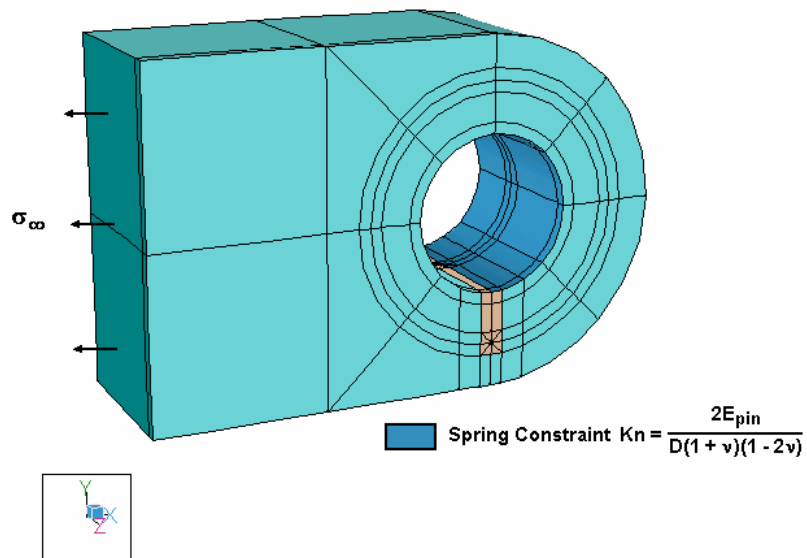


Figure 24. Lug Loading and Spring Constraints on the Hole Surface. $E_{pin} = 30,000$ ksi; $\nu = 0.3$

Table 8. Parameter Variations in Lug Models

Parameter	Description	Dimensions:
a	bore crack length, in.	$0.95T$, $1.1T$, $1.5T$, $2T$
c	surface crack length, in.	0.1407
D	hole diameter, in.	0.50
W	lug width, in.	1.0
T	lug thickness, in.	0.25
σ_{∞}	far field stress, ksi	1.0

7.3 Results

The engineering data of interest is the Mode I SIFs. The variation of the SIFs along the entire crack front, for cracks whose bore length vary from $a = 0.95T, 1.1T, 1.5T, 2T$ but with fixed surface crack length, $c = 0.1407$.

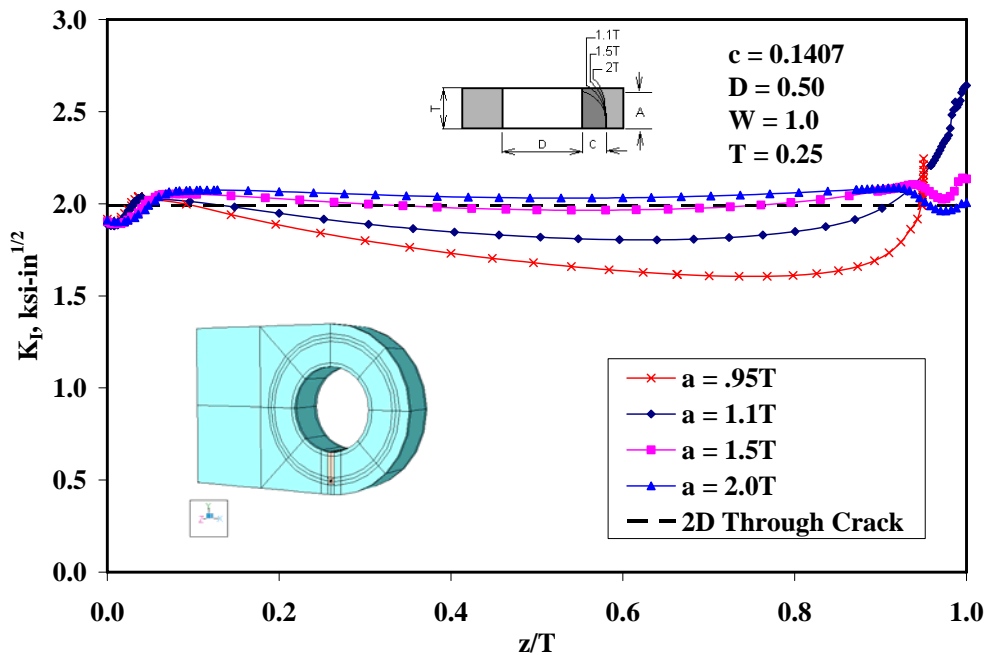


Figure 25. Stress Intensity Factors Along the Crack Front, $a = 0.95T, 1.1T, 1.5T, 2T$

Normally, the SIFs along the crack front would be plotted as a function of the elliptical angle ϕ ; however, because the crack front and the quarter ellipses do not coincide for all solutions, the x-axis in Figure 25 is the depth (z -coordinate) on the crack front normalized by the lug thickness, T . For comparison and scale in Figure 25, the 2-D through crack lug solution from a 2-D StressCheck simulation of a through crack in a lug has also been plotted. In Figure 25, the SIF

close to $z/T = 0$ is designated the surface crack SIF, while the SIF close to the last point on each curve is designated the bore crack SIF.

Starting with the smallest bore crack length in Figure 25, $a = 0.95T$, the SIF starts at about 2.0 ksi-in^{1/2}, dips down, then ramps up quickly as the bore crack tip is approached. While similar behavior is seen for all crack lengths, the variations are become less dramatic as the bore crack length is increased. The next largest crack length $a = 1.1T$ is just large enough so that the a crack tip does not intersect the bore, but intersects the lug surface on the opposite surface from the surface crack tip c and you can start to see small shifts in qualitative behavior—namely, the rise of SIF near the a crack tip is not as dramatic as for the smallest bore crack length, and the dip in SIF from $z/T = 0$ to $z/T = 0.8$ is not as dramatic as for the smallest bore crack length. As the bore crack length a increases, the SIFs flatten out and start to approach the SIFs for the 2-D through crack (solution taken from the 2-D StressCheck solution for $c = 0.1407$).

The BCF β is the normalization of the SIFs in the following function:

$$\beta \equiv \frac{K_I}{\sigma_{bear} \sqrt{\pi c}} \quad (7)$$

where: σ_{bear} is the bearing stress, defined as $\sigma_{bear} \equiv F_{pin} / (DT) = W/D$ and

F_{pin} is the force on the lug hole exerted by the pin if one were present.

While Equation (7) gives the general equation for the Boundary Correction Factors, two specific BCFs can be defined:

$$\beta_c \equiv \frac{K_{I(c)}}{\sigma_{bear} \sqrt{\pi c}} \quad (8)$$

$$\beta_a \equiv \frac{K_{I(a)}}{\sigma_{bear} \sqrt{\pi c}} \quad (9)$$

where: $K_{I(c)}$ is the SIF of the surface crack tip, near $z/T = 0$,

$K_{I(a)}$ is the SIF of the bore crack tip, near $z/T = 1$,

β_c is the BCF of the surface crack tip, and

β_a is the BCF of the surface crack tip.

Focusing on the behavior of the surface crack BCFs, the local maxima in the SIFs (and hence BCFs) near $z/T = 0$ are extracted, Table 9. Note the lug dimensions are fixed and only the elliptical crack length a varies. The table shows the effect of the change in bore crack length a on the surface crack SIF and BCF, $K_{I(c)}$ and β_c , respectively, at constant surface crack length c . While elliptical oblique crack $K_{I(c)}$, β_c values increase as the crack length a increases, the

percent change is less than 2 percent. Included in the table is the $K_{I(c)}$ value for the two-dimensional through crack solution. The BCF β_c behavior is shown in Figure 26.

Table 9. $K_{I(c)}$ and β_c for Part-Through Cracks Transitioning to Oblique Cracks

a/T	a in.	c in.	$K_{I(c)}$ ksi-in ^{1/2}	BCF β
0.95	0.2375	0.1407	2.040	1.53385
1.1	0.275	0.1407	2.036	1.53153
1.5	0.375	0.1407	2.053	1.54426
2.0	0.5	0.1407	2.075	1.56036
2-D Crack	N/A	0.1407	1.993	1.4987

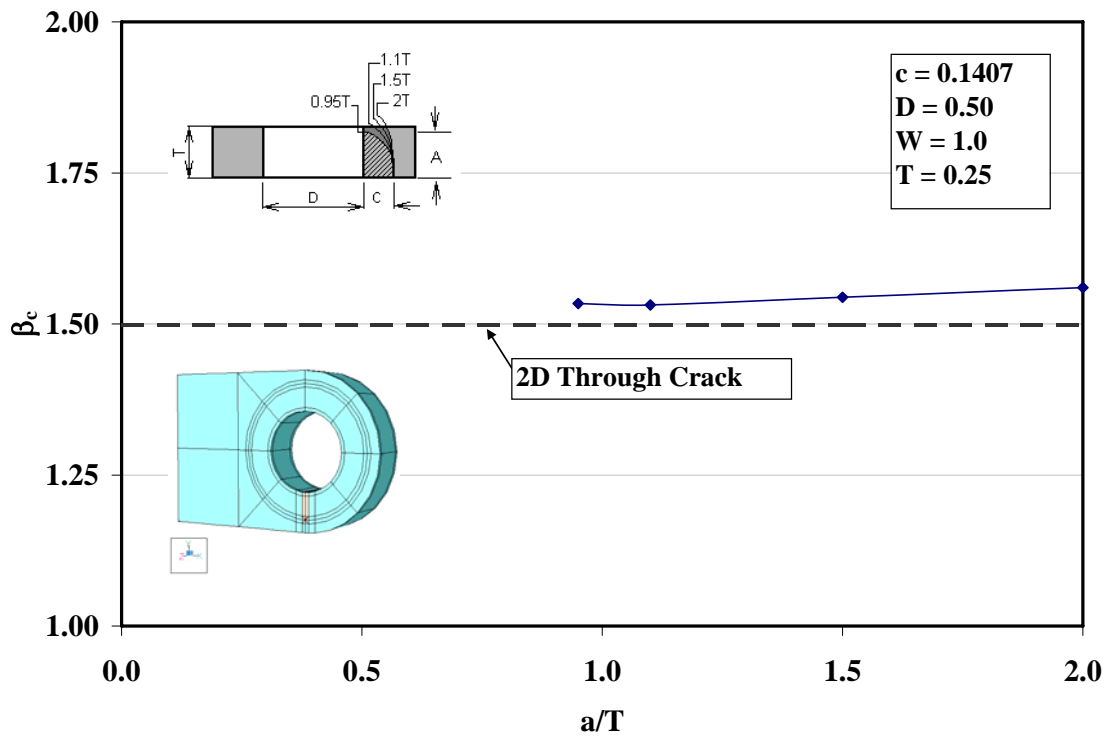


Figure 26. Behavior of β_c as a Crack Transitions from Part-Through to Oblique

It seems counterintuitive that the BCF β_c keeps increasing as the crack becomes more and more erect or straight (that is, a straight through crack is the limit as $a/T \rightarrow \infty$), the BCFs β_c should

begin to approach the BCF of the 2-D Through Crack. There are two possible reasons why this doesn't appear to be true here:

- 1) The 2-D through crack SIF is computed with a 2-D StressCheck simulation of a through crack in a lug. 2-D SIFs are independent of plane strain or plane stress assumptions; in fact, in a 3-D simulation of a single through crack at a lug, the SIFs across the straight crack front are not constant, but start lower on the surfaces, ramp up to a plateau that holds constant over most of the thickness, finally dipping down as the opposite surface is approached. The 2-D SIF will typically split the difference between the relatively low values of SIFs on the surfaces and the interior plateau that is higher than the surface SIFs. The method we use for extracting the $K_{I(c)}$ involves an analyst's judgment as to the location of a maximum local to the surface(s), effectively resulting in a $K_{I(c)}$ that is higher than the low SIFs on the surface.
- 2) A precise parallel between the computed SIFs in 2-D and 3-D does not exist; the 2-D SIFs make no assumptions about the thickness, so that plane strain and plane stress are the same. The 3-D SIF extraction in StressCheck, however, does make estimates of how close to plane strain or plane stress a location in the interior of the lug is, and the computation of the SIFs is affected accordingly.

7.4 Challenges

The modeling of an oblique crack in a 3-D finite element model is time consuming and labor intensive, if a full range of oblique crack solutions is desired, a very large computational matrix would be needed to adequately cover the full range of problem parameters. Each combination of W/D , D/T , and a/c would require at least 4 to 5 variations of a/T for $1 \leq a/T \leq \infty$.

7.5 Limitations

Because the goal of this study was to determine the qualitative behavior of the Stress Intensity Factors on a part-through crack as it transitions from a corner crack to an oblique crack, the solutions presented here fixed the surface crack length to one particular value. This limitation makes this work of little value if different parameter values are needed. However, this was an excellent study that documented the SIFs of a crack as it transitions from part-through to oblique, and should give the analyst some idea of how other transitions with a different set of parameters might progress.

7.6 Conclusions and Recommendations

7.6.1 Conclusions

Three-dimensional finite element models of lugs, each with a single crack at the corner of the hole bore, were simulated with StressCheck. The goal of the analysis was to compute accurate and reliable Mode I Stress Intensity Factors along the entirety of the crack fronts, and to use key values of the SIFs along the crack front to demonstrate crack SIF behavior as the crack transitions from a part-through crack to an oblique crack. The following conclusions from this analysis are possible:

- The SIFs of a single crack on a lug as the crack transitions from part-through to oblique

(curved through) at first jump up when the crack transitions from $a/T = 0.95$ to $a/T = 1.1$, but then drop and level off at subsequent a/T .

- The SIFs of the surface crack appear to be gradually increasing as a/T increases (at least up to $a/T = 2$), and do not appear to be asymptotically approaching the 2-D SIFs for a single through crack at a lug. While troubling, this apparent discrepancy in the asymptotic behavior can be explained by key differences between 2-D and 3-D Stress Intensity Factor calculation procedures.
- Very preliminary correlation (conducted by Mr. Nic Moyle) of 3-D distributed spring models with Purdue experimental tests indicate that the analytical K results are perhaps 15 percent to 25 percent under the experimental K values. Bearing stress loaded models provide a higher K result than do distributed spring reacted models (for identical lug geometries), so the two solutions may bracket the physical behavior of the Purdue lug tests. It is anticipated that Mr. Moyle will publish further documentation on these correlations for his M.S. thesis.

7.6.2 Recommendations

The SIFs of part-through and oblique cracks in three-dimensional lugs are important engineering data needed to perform robust damage tolerance analyses of lugs in aircraft structure. Since there is a measurable difference between oblique crack SIFs and straight through crack SIFs, damage tolerance analyses could be made more robust and reliable by construction of a large matrix of SIFs for various oblique crack aspect ratios, and then full integration with the existing set of lug solutions in crack propagation software such as AFGROW.

The appendix contains further information on the applicability of these modeling techniques to experiments.

8. Conclusions and Recommendations

8.1 Conclusions

This study has provided the opportunity to enhance practical applications for crack growth analysis using an External K-solver tightly integrated with the AFGROW software. The plug-in demonstrations illustrate that key technologies have matured enough for implementation into current damage tolerance design tools. The computation requirements normally do not necessitate machine capability beyond the reach of most users, but the present speeds and space requirements in many applications will require patience and/or tabulated solutions for practical reasons. The plug-in applications will benefit from an integrated group of experts pursuing specific problem types that are of immediate benefit, while also constructing the appropriate infrastructure to further capture the advantages of interactive solutions. This document advocates that the AFRL develop a multi-phased plan that starts with feasible solutions which produce immediate benefit to aircraft structure, then begins to build libraries of simple solutions, and continues on to meet successively more complicated structural problem classes as lessons are learned and processes formulated.

The AFGROW crack growth analysis software has developed a large and significant user base; its platform has achieved levels of confidence and credibility within the aircraft community. Damage tolerance design tools must be organized, understood, accessible, and utilized for the benefits to be fully realized by the USAF and the aircraft industry. The future evolution of integrated External K-solver—AFGROW software into such a tool must take into account specific user design systems requirements to continue to build and maintain confidence and reliability. To demonstrate that integrated External K-solver—AFGROW software can meet those user needs, a major aircraft manufacturer (the Boeing Company) has assisted in defining these system requirements. The maximized Return on Investment (ROI) for the technology resides in the tools being applied to aircraft structure in all phases: from design, through production, into service, and finally into the fleet retirement. Those applications must ensure safety, maximize readiness, and minimize cost.

Enhancements to 2-D and 3-D lug solutions can have immediate impact for the industry. Pre-engineering of the solution tables, that is, determining the acceptable parametric ranges of the models, determining which model is appropriate for which parameter space, and ensuring solution convergence and quality, is the most appropriate integration strategy for simpler problems that require rapid and easily-available solutions. The pre-engineered table lookup approach, while necessarily limited by the acceptable model parameters, will permit the industry to access these solutions in a timely fashion.

8.2 Recommendations

Building upon the external-K solver plug-in functionality described and demonstrated in this document, additional problem types and classes critical to industry should continue to be identified and implemented within the existing framework of AFGROW and StressCheck®. Using industry guidance to determine the types and the required fidelity of future models is essential for building user acceptance of the solutions.

It is also essential that discussions continue between AFRL, AP/ES, Boeing, and ESRD regarding StressCheck® licensing issues. Currently, ESRD is allowing any external-K solver user to access specific solutions using the license purchased by AFRL via AP/ES, but this agreement is only in effect while the integrated software is still in a 'prototype' mode. As the integrated software matures, we will need to jointly evaluate the StressCheck® licensing issues for the general community of external-K solver users.

The appendix contains further information on the applicability of the selected modeling techniques to experiments.

9. References

[1] APES, Inc. “Crack Growth and Stress Intensity Prediction Techniques”, Final Report for Contract F33615-98-D-3210, 31 December 2004

[2] APES, Inc. “Correlation of Analytic External K-Solutions with Boeing/Purdue Mechanical Tests (Rev. A)”, Final Report for Boeing Order #5CS2221, 23 June 2005

10. Appendix: Correlation of Experimental and Analytical Lug Stress Intensities

10.1 Introduction

After initial publication of this report, new information was received regarding Purdue experimental lug test results [Moyle, Nicholas, “Experimental Determination of the Mode I Stress Intensity Factor for a Corner Cracked Lug Using a Marker Banding Technique”, Purdue University M.S. Thesis, School of Aeronautics and Astronautics, May 2006]. After receiving feedback from several industry members and AFGROW users, most of which requested the preferred lug modeling approach (bearing stress or distributed springs), AP/ES looked into the details of Mr. Moyle’s thesis in order to determine the best modeling approach.

Purdue’s correlation of experimental test results to the analytical models determined that test results showed better agreement with the pin bearing boundary conditions for shorter corner cracks, and test results for larger corner cracks and through-the-thickness cracks agreed better with the distributed spring boundary condition.

10.2 Comparison of Bearing and Distributed Spring Boundary Conditions

Recall that the Distributed Spring model idealizes the pin-lug load transfer with normal springs distributed 180 degrees around the inside of the hole. Bearing Stress idealizes the pin-lug load transfer with a $A \cos(\theta)$ normal traction distributed 180 degrees around the inside of the hole.

Testing of these two methods for idealizing the pin-lug load transfer revealed the following trends:

- if the normal spring constant K_n , which is proportional to the Young’s modulus of the pin, E_{pin} becomes small (that is, the pin becomes very compliant), the Stress Intensity Factors (SIFs) using the two models approach each other (Table 10 below); and
- if the ratio of the lug width to pin diameter, W/D becomes large, the SIFs from the two models approach each other. See Figure 7, Chapter 2, which it is apparent that the stress distributions on the crack plane (in uncracked lugs of course) become the same for these two boundary conditions (bearing vs. springs) as W/D becomes large.

Table A-1. Convergence of SIFs for $a = 0.05$ as $W/D \rightarrow big$ and $E_{pin} \rightarrow small$

	Bearing	Springs	Springs	Springs	Springs	Springs
W/D	Stress	$E_{pin}=30000$	$E_{pin}=3000$	$E_{pin}=300$	$E_{pin}=30$	$E_{pin}=3$
	K_I	K_I	K_I	K_I	K_I	K_I
1.3	5.4967	3.0218	3.4962	4,4916	5.3308	5.5514

1.5	3,1936	1.8867	2.1874	2.7840	3.0764	3.1203
2.0	1.9206	1.4565	1.6208	1.8576	1.9181	1.9256
4.0	1.6668	1.5159	1.5977	1.6554	1.6664	1.6675
5.0	1.8006	1.6732	1.7441	1.7915	1.7994	1.8002

It appears as if the bearing stress simulates ‘well’ either a very soft pin, or a very big (relative to the hole diameter) lug.

The pin bearing boundary condition consistently produces higher Mode I Stress Intensity Factors than does the distributed spring boundary condition when a steel pin modulus is assumed. As the assumed pin modulus and spring stiffness becomes softer, the Stress Intensity Factors increase until they approach the bearing boundary condition results. A probable reason for this is the ‘hole propping’ effect: a stiff pin restrains the deformation of the lug more than a soft pin, lowering both the local stresses and the local Stress Intensity Factors.

10.3 Pin-to-Lug Fitting Effects

All analytical results presented in the body of this report, for both the bearing B.C. and the distributed spring B.C. assumed a ‘neat-fit’ pin, which assumes that the pin and the lug hole diameters are identical. Of course, exactly equal diameters are impossible to achieve in practice, and detailed in Mr. Moyle’s thesis are the physical measurements of the pin and the lug holes. Although achieving neat-fit pins was one goal of the Purdue experiments, the specified machine tolerance on the lug holes was $-0.000/+0.003$ ” of the pin diameter, and physical measurements of all specimens yielded a maximum gap between the pin and the lug of 0.002 ”. This maximum gap value of 0.002 ” was examined in StressCheck®, using the fastener element, to determine its effect on the Stress Intensity Factors.

Results of this examination are shown in Figure 27 for two different crack sizes, 0.005 ” and 0.05 ”. The upper curve is for the 0.05 ” crack size. The 2-D tabulated bearing and distributed spring solutions from the body of this report are also shown for comparison. As expected, the distributed spring boundary condition results are nearly identical to the neat-fit fastener element results when a steel pin modulus is assumed. Also as expected, the bearing boundary condition Stress Intensity Factors are consistently higher, and are consistent with pin clearances in the interval -0.001 ” to -0.0005 ”.

Clearly, even a moderate pin clearance of 0.001 inch can have a significant (~40 percent) effect on the Stress Intensity Factors. The effect of a small amount of ‘slop’ in the fit of the pin to the lug can easily be more significant than the effect caused by choice of boundary condition for the model. The bearing boundary condition can help to approximate the higher initial Stress Intensity Factors if there is a less-than-perfect fit of the pin to the lug.

10.4 Recommendations for AFGROW Users

One potential reason why Purdue’s test results are better modeled by the bearing boundary condition for smaller cracks is because the physical fit of the pin is not perfect, which leads to no ‘hole propping’ effect initially. The experimental Stress Intensity Factors are higher than if the

experiments had achieved a truly ‘neat-fit’ pin, and using the analytical bearing boundary condition helps to capture this effect. As the crack gets longer (on the order of 0.1” and larger) and the lug deforms more, the steel pin then begins to contact and ‘prop’ the hole, reducing the Stress Intensity Factors, and so the analytical results begin to match the analytical distributed spring boundary condition better.

A possible recommendation to AFGROW users is to assume the bearing stress boundary condition to provide a conservative result, especially if one is unsure that a true neat-fit has been achieved. If there is an excellent fit of the pin to the hole, or even a slight interference fit, then the distributed spring boundary condition is probably a better choice.

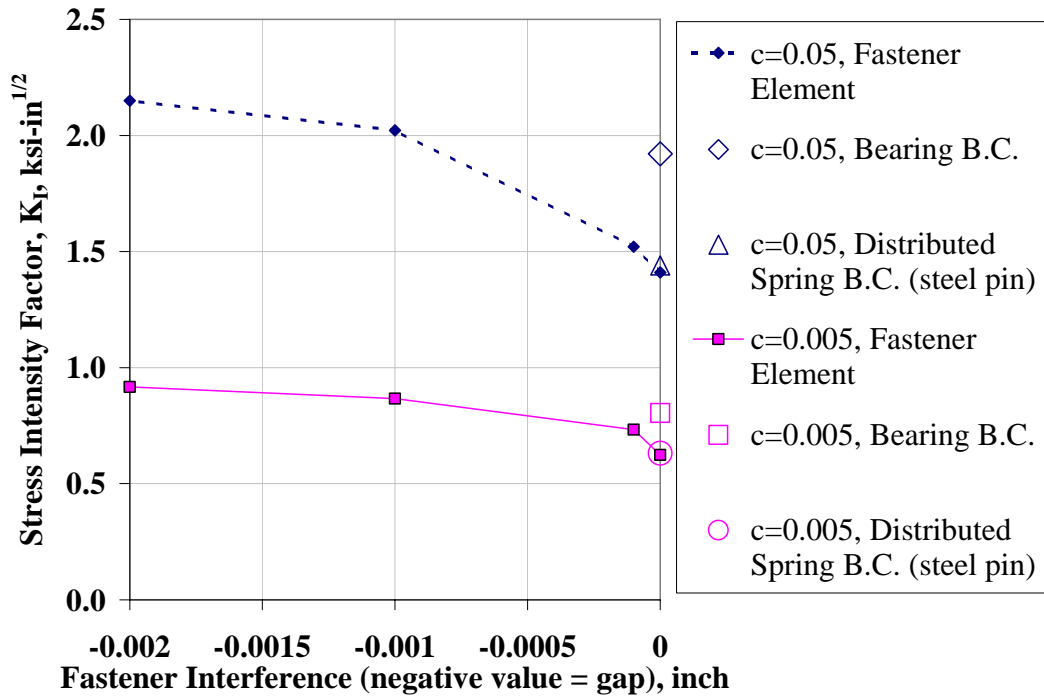


Figure A-1. 2-D Stress Intensity Factors for $W/D=2$, $\sigma_{ff}=1$, $\sigma_{brg} = 2$